Isotopic Evidence for Mercury Photoreduction and Retention on Particles in Surface Waters of Central California, USA

Spencer J. Washburn[1,a,*], Joel D. Blum[1], Patrick M. Donovan[1], and Michael Bliss Singer[2,3,4]

[1] Department of Earth and Environmental Sciences, University of Michigan, Ann Arbor, Michigan 48109, United States

[2] School of Earth and Ocean Sciences, Cardiff University, Cardiff CF10 3AT, United Kingdom

[3] Water Research Institute, Cardiff University, Cardiff CF10 3AX, United Kingdom

[4] Earth Research Institute, University of California Santa Barbara, Santa Barbara, CA 91306, United States

[a] Present Address: Smithsonian Environmental Research Center, 647 Contees Wharf Road, Edgewater, Maryland 21037, United States

Abstract:

Cache Creek (Coast Range, California) and the Yuba River (Sierra Nevada Foothills, California) are two river systems affected by extensive mercury (Hg) contamination due to legacy sources of Hg related to mining. Stable Hg isotope techniques have proven useful for elucidating the complex cycling of Hg within aquatic ecosystems, and we applied these techniques to improve understanding of Hg and methylmercury (MeHg) transformations in these watersheds. Total mercury (THg) concentrations and Hg stable isotope ratios were measured in filtered surface waters and suspended particulate matter collected from 14 sites within the Cache Cr. and Yuba R. watersheds. Filtered surface waters from both watersheds exhibited values of Δ^{199}Hg (0.37‰ to 0.71‰), consistently elevated above those observed in sediments (Δ^{199}Hg average = 0.07‰). Associated suspended particulates from these surface water samples displayed a much greater range of values for Δ^{199}Hg (-0.61‰ to 0.70‰), although suspended particulates from the Yuba R. exhibited mostly negative Δ^{199}Hg values (-0.61‰ to 0.10‰). The relationship between Δ^{199}Hg and Δ^{201}Hg in the filtered surface waters and associated suspended particulates was calculated using a bivariate York regression, yielding a slope of 1.57±0.49 (±2SE) for the Yuba R. and 1.40±0.27 (±2SE) for Cache Cr., both within error of the previously reported experimentally-derived slopes for MeHg- and inorganic Hg(II)- photoreduction. This

provides isotopic evidence that Hg photoreduction is occurring within these surface waters to a significant degree, and suspended particulate phases are retaining the reduced product of Hg photoreduction, particularly within the Yuba R. The isotopic compositions of filtered surface waters are consistent with the isotopic signatures recorded in biota at low trophic positions within these watersheds, suggesting that the reservoir of Hg incorporated within the biota of these systems is similar to the filter-passing Hg fraction in surface waters.

Keywords: mercury; stable mercury isotopes; mercury photoreduction; contaminated fluvial ecosystem

1. Introduction

Historic mining activities in the watersheds of numerous Central Valley, California rivers have resulted in an enduring legacy of widespread mercury (Hg) contamination throughout the region. In the Sierra Nevada foothills, hydraulic gold mining activities in the nineteenth century mobilized immense amounts of Hg-contaminated sediment into the downstream portions of rivers like the Yuba River, and the effects of these activities continue to impact river function and ecosystem health both locally and far downstream (Domalgalski, 2001; Marvin-DiPasquale et al., 2003; Domalgalske et al., 2004; Alpers et al., 2005; James et al., 2009; Bouse et al., 2010; Ghoshal et al., 2010; Fleck et al., 2011; Marvin-DiPasquale et al., 2011 Springborn et al., 2011; Donovan et al., 2013; Singer et al., 2013; Higson and Singer, 2015; Singer et al., 2016; Nakamura et al., 2018). In the California Coast Range, Hg-ores have been mined since the mid-nineteenth century to produce metallic Hg, creating substantial contamination related to release of Hg from the retorting process and mine waste tailings in the rivers that drain these areas, such

as Cache Cr. (Domalgalski et al., 2004 USGS; Marvin-DiPasquale et al., 2009; Suchanek et al., 2010). Coast Range watersheds also experience continuing inputs of Hg from natural processes related to hydrothermal activity and leaching from Hg-containing outcrops (Smith et al., 2008 and references therein; Suchanek et al., 2010). The continuing impacts of this widespread contamination on biota in these systems, as evidenced by elevated methylmercury concentrations, has been well documented for both aquatic and terrestrial organisms (May et al., 2000 USGS; Alpers et al., 2004 USGS; Hothem et al., 2007; Hothem et al., 2008; Hothem et al., 2010; Fleck et al., 2011 USGS) and extends downstream into the San Francisco Estuary (Eagles-Smith et al., 2009; Greenfield & Jahn, 2010; Donovan et al., 2013). There is, however, a significant knowledge gap within the field of Hg biogeochemistry as to how elevated sources of inorganic mercury (IHg), such as the legacy mining sources affecting the Yuba R. and Cache Cr. watersheds, correspond to and affect methylation of Hg and subsequent bioaccumulation within organisms (Domagalski et al., 2004).

More specifically, there are still open questions about the transformation of aqueous Hg species into the bioavailable pool of Hg within freshwater fluvial ecosystems (Ward et al., 2010). Stable Hg isotope studies have emerged within the last decade that demonstrate the ability of this method to elucidate the complex transformations Hg undergoes during environmental cycling (Yin et al., 2010; Blum et al., 2014; Blum & Johnson, 2017). Specifically, Hg isotopes have been used within California river systems to study the relationship between sediment-associated Hg and concentrations of Hg within invertebrates and fish (Donovan et al., 2016a; Donovan et al., 2016b). These studies identified distinct MeHg and IHg isotope endmembers within the study watersheds, but have been unable to identify specific processes that could link these two endmembers. Analysis of the specific isotopic shifts between IHg and MeHg led investigators to

78 suggest that two processes, photoreduction of MeHg and biotic fractionation (a balance of
79 methylation and demethylation processes), were necessary to explain the Hg isotopic
80 composition of biota. Experimental studies of photochemical reduction of both IHg and MeHg
81 have demonstrated that these processes impart characteristic odd mass independent fractionation
82 (MIF) signatures (Bergquist and Blum, 2007; Zheng and Hintelmann, 2009; Chandan et al.,
83 2015; Rose et al., 2015), but the limited number of field studies conducted in freshwater aquatic
84 ecosystems to date have focused on the isotopic composition of receptor organisms (e.g.
85 macroinvertebrates, fish) rather than abiotic Hg pools (Tsui et al., 2013; Kwon et al., 2015;
86 Lepak et al., 2018).
87 Using stable Hg isotope analysis, this study builds upon previous research by
88 investigating the transformation of Hg within surface waters, particularly photoreduction
89 processes, to understand the role these species play in the isotopic shifts associated with
90 transformation of IHg to bioavailable forms. California surface waters exhibit significant odd
91 MIF anomalies, providing isotopic evidence that photoreduction processes are actively affecting
92 Hg cycling in these fluvial systems. California surface waters also display isotopic compositions
93 that are consistent with the isotopic compositions of low trophic position biota within these
94 watersheds, providing evidence that the reservoir of bioavailable MeHg is also present in the
95 surface water pool.
96 **2. Materials and Methods**
97 **2.1 Sample Collection and Processing**
98 Filtered stream water and suspended sediment samples were collected at fifteen locations
99 along the Yuba R. (including the Feather River downstream of the confluence with the Yuba R.),
100 Cache Cr. (including Bear Creek and Sulfur Creek in the headwater regions of Cache Cr.), and

101 the Yolo Bypass Wildlife Area (YBWA) during June 2015 (06/02/15 to 06/09/15). Sampling
102 locations within each watershed were chosen to align with sites at which samples had been
103 previously collected and analyzed for Hg isotopic analysis by Donovan et al. (2016a) and
104 Donovan et al. (2016b) (Figure S6). Water samples ranging from 1 L to 15 L in volume were
105 collected, filtered, and preserved in the field, using trace-metal clean sampling methods
106 following a modification of EPA Method 1669. All filtered water field blanks (n=8) had THg
107 concentrations that were below method detection limits of 0.2 ng/L. At each site, 1L of water
108 was collected into a HDPE bottle and used to determine the total suspended solids (TSS) of
109 surface water. TSS values were used in the calculation of distribution coefficients ($\log K_d$) using
110 THg values of the associated filtered surface water and suspended material following the method
111 of Hurley et al. (1998).

112 **2.2 Sample Preparation for Isotope Analysis and THg Concentrations**

113 Hg in suspended material was separated for THg concentration and Hg stable isotope
114 measurement by offline combustion, as described in detail elsewhere (Biswas et al., 2008;
115 Demers et al., 2013). Hg in filtered surface water was separated for Hg stable isotope
116 measurement by adsorption onto an anion exchange resin (AG-1X4, Biorad, 200-400 mesh)
117 using a method modified from the procedure described in Štrok et al. (2014) and detailed in the
118 unabridged methods [SI S1]. Prior to anion exchange, THg concentrations of each surface water
119 sample were determined by analysis of small aliquots of UV-treated samples via CV-AFS
120 (following EPA method 1631). Recovery of filtered surface water samples during the anion
121 exchange resin column process averaged 91.6% ± 3.1% (range: 86.2% to 95.5%, n=7). Three
122 samples with suspected high DOC contents had poor recoveries (YBWA PW#2, 4.1%; Rumsey,
123 Cache Cr, 58.8%; Bear Cr. @HCC, 47.9%); the mass independent isotopic composition of

samples is unchanged by incomplete yields, but the mass dependent isotopic composition may have been affected. Therefore, although reported in this manuscript, the mass dependent isotopic composition of these samples is suspect, and the Δ^{xxx}Hg values of these low-recovery samples are displayed in manuscript figures and tables with an asterisk. While not an exhaustive investigation, these low sample yields of Hg suggest that the anion exchange resin column method may not be the ideal pre-concentration protocol for low Hg concentration waters with high DOC contents.

Trapping solutions of both combustion and column resin-exchange samples were partially reduced with a 30% solution of $NH_2OH{\cdot}HCl$ using an amount equal to 2% of the total sample by weight (w/w); then a small aliquot was taken and measured for THg by CV-AFS or cold vapor atomic absorption spectroscopy [CV-AAS; MA-2000 Nippon Instruments]. Combustion trap contents and surface water eluents were then purged into a secondary 1% $KMnO_4$ trapping solution to remove potential matrix components and to adjust Hg concentrations prior to isotopic analysis (Sherman and Blum, 2013; Blum and Johnson, 2017). Transfer recoveries into secondary traps for concentration and matrix- matching for all sample types averaged 96.8% ± 5.8% (range: 73.3% to 106.6%, n=42, only 2 transfers <85% recovery). None of these transfers are likely to have significantly fractionated the processed samples (Blum and Johnson, 2017).

Procedural blanks were processed in parallel with samples for THg concentration and Hg isotopic composition. The trap contents of combusted field filter blanks contained 104±18 pg of Hg (n=8, ± 1SD), which is not significantly different from procedural combustion blanks (105±74pg of Hg, n=10, ± 1SD). Column resin-exchange procedural blanks yielded between 119 and 191 pg of Hg (n=4, mean±1SD = 149±30pg), representing no more than 5.6% of Hg in

147 sample eluent solutions.

148 **2.3 Hg Isotope Analysis**

149 The Hg isotopic composition of the secondary trapping solutions were measured by cold
150 vapor multi-collector inductively coupled plasma mass spectrometry (CV-MC-ICP-MS) at either
151 the University of Michigan (Nu Instruments) or the University of Toronto (Thermo Fisher
152 Neptune Plus). Mercury stable isotope compositions are reported throughout this paper in permil
153 (‰) using delta notation (δ^{xxx}Hg) relative to NIST SRM 3133 (Eq. 1), with mass dependent
154 fractionation based on the ^{202}Hg/^{198}Hg ratio (δ^{202}Hg) (Blum and Bergquist, 2007). Mass
155 independent fractionation is reported as the deviation from the theoretically predicted δ^{xxx}Hg
156 values based on the kinetic mass fractionation law and is reported with capital delta notation
157 (Δ^{xxx}Hg) according to Eq. 2. In this study MIF is represented with Δ^{199}Hg, Δ^{200}Hg, Δ^{201}Hg, and
158 Δ^{204}Hg, using $\beta = 0.252$, $\beta = 0.502$, $\beta = 0.752$, and $\beta = 1.493$, respectively (Blum and Bergquist,
159 2007).

160 Equation 1: $\delta^{xxx}\text{Hg}\ (‰) = ([(^{xxx}\text{Hg}/^{198}\text{Hg})_{\text{Sample}} / (^{xxx}\text{Hg}/^{198}\text{Hg})_{\text{NIST3133}}] - 1) \times 1000$

161 Equation 2: $\Delta^{xxx}\text{Hg}\ (‰) = \delta^{xxx}\text{Hg} - (\delta^{202}\text{Hg} \times \beta)$

162 Certified reference materials and standards were processed and analyzed along with the
163 California water samples. UM-Almáden was used as the process reference material for the
164 column resin exchange procedures. Column anion exchange resin recoveries for UM-Almáden
165 averaged 97.3% ± 3.7% (range: 93.3% to 101.7%, n=4). NIST 2711 “Montana Soil,” was chosen
166 as a suitable process reference material for offline combustions due to its high THg conc.
167 (6.25µg/g) and similar matrix. Combustion recoveries of NIST 2711 averaged 102.3% ± 5.8%
168 (range: 92.6% to 108.9%, average THg conc = 6391± 365 µg/g, n=8). The average isotopic
169 composition of NIST 2711 (δ^{202}Hg= -0.25 ± 0.10‰, Δ^{199}Hg= -0.27 ± 0.03‰) was consistent

with previously reported values (Estrade et al., 2011; Jiskra et al., 2015; Yin et al., 2016; Blum and Johnson, 2017; Washburn et al., 2017; Washburn et al., 2018a; Washburn et al., 2018b). UM-Almáden was measured during each analytical session on the CV-MC-ICP-MS to quantify within-session performance. The isotopic data from these process reference materials and process standards is summarized in Table S1. The analytical uncertainty of Hg isotopic measurements (2SD) is presented regardless of sample preparation method used, because the error associated with the 2SD of UM-Almáden (averaged across analytical sessions) was greater for all measured Hg isotope values than that associated with the sample matrix specific process reference material (2SE). Hence, the analytical uncertainty of Hg for samples in this study is presented as δ^{202}Hg ± 0.12‰, Δ^{199}Hg ± 0.03‰, Δ^{201}Hg ± 0.08‰, Δ^{200}Hg ± 0.05‰ and Δ^{204}Hg ± 0.20‰. [Table S1].

3. Results and Discussion

3.1 Isotopic Composition of Hg in California Surface Waters

Filtered surface waters collected from the Yuba R. and Feather R. displayed low THg concentrations (0.48 to 0.86 ng/L), and relatively small variation in isotopic composition (δ^{202}Hg = -0.82‰ to -0.50‰, avg. = -0.69±0.13 ‰ [1SD]; Δ^{199}Hg = 0.37‰ to 0.62‰, avg. = 0.49±0.14 ‰ [1SD]) [Table 1; Figure 1]. The associated suspended particulates displayed a much greater range in both THg concentrations (166.1 to 665.2 ng/g) and isotopic composition (δ^{202}Hg = -1.31‰ to 0.25‰, avg. = -0.68 ± 0.54‰ [1SD]; Δ^{199}Hg = -0.61‰ to 0.10‰, avg. = -0.21 ± 0.24‰ [1SD]) [Table 1; Figure 1]. Both filtered surface waters [Unpaired t-Test with equal variance, n_1=4, n_2=12, T=11.40, p<<0.001] and suspended particulates [Unpaired t-Test with equal variance, n_1=6, n_2=12, T=3.731, p=0.003] have significantly different average Δ^{199}Hg values than Yuba R. riverbank and terrace sediments (Δ^{199}Hg = 0.04 ± 0.03 ‰ [1SD]) (Donovan

et al., 2016a).

Filtered surface waters collected from Cache Cr. and Bear Cr. (which flows into Cache Cr.) displayed relatively low THg concentrations (1.03 to 11.78 ng/L), and relatively limited variation in isotopic composition (δ^{202}Hg = -0.84‰ to -0.73‰; Δ^{199}Hg = 0.58‰ to 0.64‰).This small range likely reflects the low number of data points analyzed for Hg isotope composition (n=2) [Table 1; Figure 2]. Similar to the Yuba R., the associated suspended particulates displayed a much greater range in both THg concentration (114.6 to 2788 ng/g) and isotopic composition (δ^{202}Hg = -1.78‰ to -0.91‰, avg. = -1.23 ± 0.30‰ [1SD]; Δ^{199}Hg = 0.05‰ to 0.53‰, avg. = 0.19 ± 0.17‰ [1SD]) although this greater range may be influenced by the greater number of suspended particulate samples analyzed for Hg isotope composition (n=7) [Table 1; Figure 2]. Unlike the Yuba R., Cache Cr. suspended particulates did not have a significantly different average Δ^{199}Hg value compared to riverbed and terrace sediments (Δ^{199}Hg = 0.10 ± 0.06‰ [1SD]) [Unpaired t-Test with equal variance, n_1=7, n_2=14, T=1.804, p=0.087] (Donovan et al., 2016b). Filtered surface waters from Cache Cr. displayed Δ^{199}Hg values that were significantly elevated compared to sediments [Unpaired t-Test with equal variance, n_1=2, n_2=14, T=267, p<<0.001]. Filtered surface water and suspended particulates collected from Sulfur Creek displayed the greatest THg concentration (179.1 ng/L), the most negative δ^{202}Hg values (-2.47‰ and -2.89‰, respectively) and the most positive Δ^{199}Hg values (0.71‰ and 0.70‰, respectively) of any surface waters analyzed in this study [Figure 2, Table 1].

3.2 Isotopic Evidence for Mercury Photoreduction in Surface Waters

3.2.1 Δ^{199}Hg/Δ^{201}Hg Ratio in Surface Waters

Filtered surface waters from both watersheds exhibited consistently elevated Δ^{199}Hg values (0.37‰ to 0.71‰) and Δ^{201}Hg values (0.21‰ to 0.51‰) (Figure 4; Table 1). The

associated suspended particulates from these surface waters displayed a much greater range of Δ^{199}Hg values (-0.61‰ to 0.70‰) and Δ^{201}Hg values (-0.38‰ to 0.50‰), but a number of particulate samples had negative MIF values, suggesting suspended particulates may be affected by a different set of fractionation processes, or are retaining a different phase of Hg than filtered surface waters (Figure 3, Figure 4, Figure S1, Figure S5, Table 1).

Previous experimental studies have established that the Δ^{199}Hg/Δ^{201}Hg ratio of samples can be diagnostic of the occurrence of specific fractionation processes, including photochemical reduction reactions (Bergquist & Blum, 2007; Zheng & Hintelmann, 2009; Rose et al., 2015; Chandan et al., 2015). If a singular fractionation mechanism was responsible for the odd mass-independent isotopic compositions of the CA surface waters, one would expect that they would exhibit characteristic Δ^{199}Hg/Δ^{201}Hg ratios in good agreement with one of the previously determined experimental slopes for MIF inducing mechanisms. Regression statistics for the relationship between Δ^{199}Hg/Δ^{201}Hg in the filtered surface water and associated suspended particulates of each river were calculated using the Model 2 bivariate York regressions embedded in *Isoplot* (v.3.00, Ludwig) [Figure 4] and found to be 1.57±0.49 (±2SE) for the Yuba River and 1.40±0.27 (±2SE) for Cache Creek. Applying the same regression model to the entire surface waters dataset presented in this manuscript yields a slope that is statistically indistinguishable from the slopes calculated for the rivers individually: 1.52±0.24 (±2SE) (Figure 4). The Δ^{199}Hg/Δ^{201}Hg slopes for each river overlap with a number of previously reported, experimentally-derived slopes. These include MeHg photo-reduction with a slope of 1.36±0.08 (±2SE) (Bergquist and Blum, 2007), photoreduction of Hg(II) at environmentally relevant Hg/DOC ratios with slopes ranging from 1.19 ±0.02 to 1.31±0.14 (±2SE) (Zheng & Hintelmann, 2009), and an experimentally-derived slope of 1.59±0.05 (±2SE) for nuclear volume effects

239 (NVE)-related fractionation associated with processes such as abiotic reduction by DOM (Zheng
240 and Hintelmann, 2010). Given that each river as well as the overall surface water dataset is
241 potentially consistent with a number of MIF-inducing mechanisms, it is possible that odd-MIF
242 isotopic composition of surface waters in these rivers may not be controlled by a single process.
243 If just considering filtered surface water samples, the calculated $\Delta^{199}Hg/\Delta^{201}Hg$ York
244 regression slope of 1.13±0.32(±2SE) is significantly lower than the overall dataset slope. Filtered
245 surface water samples exhibit MIF isotopic compositions that are consistent with both MeHg
246 photoreduction and photoreduction of Hg(II) at environmentally relevant Hg/DOC ratios (Zheng
247 & Hintelmann, 2009; Bergquist and Blum, 2007; Chandan et al., 2015). Photoreduction of both
248 MeHg and Hg(II) can produce the relatively large magnitude MIF anomalies observed in the
249 filtered surface water samples ($\Delta^{199}Hg$ values up to 0.71‰) with much smaller MDF shifts.
250 Although not directly measured in this study, MeHg concentrations in filtered surface waters of
251 the Yuba R. and Cache Cr. watersheds have previously been demonstrated to be low, with MeHg
252 concentrations typically <<1ng/L and representing <10% of THg of these surface waters
253 (Domalgalski et al., 2004 USGS; Hunerlach et al., 2004; Stumpner et al., 2018). Despite the low
254 MeHg concentrations, the odd-MIF signatures of Hg in the surface waters of these watersheds
255 suggests that the Hg remaining in these surface waters is partially influenced by MeHg
256 photoreduction processes. A combination of these two photoreduction processes, acting on IHg
257 and MeHg reservoirs with slightly different starting MIF isotopic compositions, could produce
258 the observed $\Delta^{199}Hg/\Delta^{201}Hg$ ratio in the surface waters we have analyzed (Figure S5).
259 The large degree of uncertainty in the calculated regression $\Delta^{199}Hg/\Delta^{201}Hg$ slope for
260 filtered surface waters could be driven by differences in the starting isotopic composition of pre-
261 photodegraded Hg (either MeHg or inorganic Hg(II)) between the two watersheds, as well as

spatial variations within each watershed. Previous studies have suggested that the differences in the isotopic composition of pre-photodegraded MeHg could be related to contrasting net biotic fractionation (a balance between biotic methylation and demethylation processes) between sites, or the large range in IHg source isotopic composition observed in these two watersheds (Donovan et al., 2016a; Donovan et al., 2016b). Neither filtered surface waters nor suspended particulates exhibit significant longitudinal trends in Δ^{199}Hg values along the sampling transects in the Yuba R. or Cache Cr. (Fig. S3). In both watersheds there is sufficient variation in suspended particulate Δ^{199}Hg values between adjacent sampling locations such that the transport of particulates downstream could influence the overall isotopic composition in downstream filtered surface water samples if sufficient exchange of Hg occurred between these phases.

The Δ^{199}Hg/Δ^{201}Hg slope of filtered surface waters [1.13±0.32(±2SE)] does not agree with the experimentally derived slope for NVE-related MIF [1.59±0.05 (±2SE)], but including the particulate samples in the Δ^{199}Hg/Δ^{201}Hg slope linear regression shifts the regression slopes for each river to within error of NVE effects. As the filtered surface water and suspended particulate Hg phases are likely undergoing parallel fractionation processes, it is possible that the MIF anomalies observed in filtered surface waters are partially created by NVE-related processes. However, NVE has only been observed to produce small odd-MIF signatures of ≤ +0.40‰ in simulated natural systems (Zheng & Hintelmann, 2010), which is less than the magnitude observed in the surface water samples (Δ^{199}Hg up to 0.71‰). Importantly, NVE-related shifts in Δ^{199}Hg would also impart much larger shifts in δ^{202}Hg values for the filtered surface waters (shifts up to ~4.00‰), and such shifts are not observed in any of the filtered surface water samples – the greatest δ^{202}Hg shift observed for any filtered surface water sample from the river sediment average is -0.44‰ (Simpson Bridge site). Hence, it is unlikely that NVE-

related processes are responsible for the observed $\Delta^{199}Hg/\Delta^{201}Hg$ ratio in surface waters or are driving the large magnitude odd-MIF anomalies.

Suspended particulate samples from both watersheds are in general agreement with the $\Delta^{199}Hg/\Delta^{201}Hg$ slope values predicted for the individual river sample sets, indicating that the odd-MIF signatures of Hg within these samples is partially produced by the same photoreduction fractionation process. Suspended particulates collected from sites within the Yuba R. watershed exhibit mostly negative odd-MIF signatures ($\Delta^{199}Hg$ = -0.61‰ to 0.10‰, mean = -0.21±0.24‰ [±1SD]), while associated suspended particulates collected from the Cache Cr. watershed exhibit consistently positive odd-MIF signatures ($\Delta^{199}Hg$ = 0.05‰ to 0.53‰, mean = 0.19±0.17‰ [±1SD]). The different signs of the odd-MIF anomalies of suspended particulates for Yuba R. versus Cache Cr. suggests that there are differences in the photochemical processing of Hg within the two watersheds.

3.2.2 Retention of Hg Photodegradation Products on Suspended Particulates

In the Yuba R., suspended particulate phases appear to be retaining the reduced product of MeHg and Hg(II) photoreduction, as this reduced product would have significantly more negative $\Delta^{199}Hg$ values than the starting MeHg/Hg(II) pool (Zheng & Hintelmann, 2009). Retention of photoreduced Hg(0) could be occurring due to oxidation and subsequent aqueous sorption either on or within the particles. Direct oxidation of Hg(0) by reduced DOM under anoxic conditions has been observed experimentally (Gu et al., 2012), and such reduction could be occurring within anoxic microenvironments of particulate organic matter aggregates (Böckelmann et al., 2000; Ortiz et al., 2015). A recent study by Zheng et al., (2018), demonstrated experimentally that the Hg(II) fraction produced during oxidation by organic matter is shifted to slightly more negative $\Delta^{199}Hg$ values (~ -0.20‰) than the starting Hg(0)

reservoir due to NVE-related effects. Hence, the oxidation of photoreduced Hg(0) would enhance the negative MIF signatures within the suspended particulate phase by further shifting the isotopic composition of the retained Hg fraction to more negative odd MIF values (Figure S5).

Other processes could also be contributing to the negative Δ^{199}Hg values observed in Yuba R. suspended particulates. Soils in the watershed of the Yuba R. have been shown to have slightly negative Δ^{199}Hg values (Δ^{199}Hg= -0.1 to -0.06‰) (Zheng et al., 2016). If a significant portion of the Hg pool found in suspended particulates is sourced from watershed inputs of Hg associated with allocthonous organic matter, this could result in slightly negative Δ^{199}Hg values (Jiskra et al., 2017), but probably not of the magnitude observed in the Yuba R. samples. Such mixing would also result in shifts to lower δ^{202}Hg values that are not observed in suspended particulates, making this explanation unlikely. Abiotic reduction of Hg(II) by organic matter associated with the suspended particulates would result in the Hg(II) retained on the particulates to be shifted to more negative Δ^{199}Hg values, with a shift on the order of -0.20‰ to -0.60‰ (Zheng and Hintelmann, 2010). Abiotic reduction of Hg(II) could be contributing to the overall isotopic signature within suspended particulates, although it is unlikely that is the major process contributing to the negative odd MIF signatures of Yuba R. suspended particulates because relatively large magnitude MIF shifts would also induce a significantly larger magnitude positive MDF shift (up to ~ +5.50‰) that was not observed in suspended particulate samples. Another process that could result in negative Δ^{199}Hg values is oxidation of elemental Hg present in the sediment fraction as a result of past mining activity, although a large pool of Hg(0) would need to be present in the surface waters to create an observable shift in odd MIF signatures.

The consistently positive Δ^{199}Hg values in Cache Cr. suspended particulates contrasts

with observations from the Yuba R. One explanation for this difference is that riverbed and terrace sediments in Cache Cr. (sediments represent the largest source of IHg to surface waters in the channel) have significantly more positive Δ^{199}Hg values on average (0.10±0.06‰ [±1SD]) than those observed in the Yuba R. (0.04±0.03‰ [±1SD]) [Unpaired t-Test with equal variance, n_1=12, n_2=14, T=2.87, p<0.01] (Donovan et al., 2016a; Donovan et al., 2016b). Suspended particulates may be retaining photoreduced Hg with negative Δ^{199}Hg values, but this signal is diluted after mixing with IHg that has positive Δ^{199}Hg values. Another possible explanation for the more positive Δ^{199}Hg values in Cache Cr. suspended particulates is that retention of photoreduced Hg is more limited in Cache Cr, perhaps due to differing composition of particles within the system (e.g. differing mineral compositions with lower affinity for Hg sorption, lower density of thiol-like binding sites within organic matter substrates, more limited aggregation of particles). If the pool of Hg being photoreduced in Cache Cr. is predominantly bound to S-bearing ligands within organic matter complexes, experimental work suggests that the produced Hg(0) would actually have positively shifted Δ^{199}Hg values, which if retained would result in a Δ^{199}Hg value in the suspended particulates that was positively shifted compared to the associated sediments (Zheng and Hintelmann, 2010). Zheng and Hintelmann (2010) showed, however, that Hg bound to bulk dissolved organic matter did not exhibit the MIF signatures associated with lower molecular weight S-bearing organic complexes, suggesting that MIF related to photoreduction of S-bearing organic compounds may be a relatively limited process in the Cache Cr. watershed.

Four suspended particulate samples from Cache Cr. have Δ^{199}Hg values that are more positive than the riverbed and terrace sediment average. For these samples, largely located near headwater Hg sources associated with hydrothermal and mining activity, the MIF signatures of

suspended particulates likely represents the predominance of the source contributions. Additionally, mixing with IHg sourced from the hydrothermal and mining activities in the headwaters may have resulted in a more positive Δ^{199}Hg value in pre-photodegraded MeHg and Hg(II), particularly for samples collected from Bear Cr.

3.2.3 Extent of Mercury Photoreduction Processes

The degree to which MeHg or inorganic Hg(II) has been photodegraded within a given sample can be calculated from the isotopic composition of that sample by assuming a starting isotopic composition of the MeHg/Hg(II) pool subject to prior photochemical degradation. The average Δ^{199}Hg value within sediment from each watershed (Yuba R. Δ^{199}Hg = 0.04±0.03‰; Cache Cr. Δ^{199}Hg = 0.10±0.06‰; compiled from Donovan et al., 2016a and Donovan et al., 2016b) can be used as the starting isotopic composition of both pre-photodegraded MeHg and Hg(II), because the net biotic processes that produce MeHg do not induce MIF (Kritee et al., 2009; Rodriguez-Gonzalez et al., 2009). By assuming that all MIF is related to MeHg photodegradation and subtracting the sediment average Δ^{199}Hg values from those observed in the filtered surface waters, the total magnitude of Δ^{199}Hg shift related to MeHg photodegradation can be estimated. Calculated Δ^{199}Hg shifts range from Δ^{199}Hg = 0.33 to 0.61‰ for the Yuba R. and Cache Cr. watersheds. Since DOC concentrations in both watersheds are typically between 1-5 mg/L (Chow et al., 2007; Domalgalski et al., 2004), experimental data for isotopic fractionation of MeHg during photodegradation in the presence of 1mg/L DOC, was used to estimate the proportion of MeHg in the filtered surface waters subject to photodegradation prior to incorporation in the water column (Bergquist & Blum, 2007). These calculations show that between 10% and 17% of the total mass of Hg in the filtered surface water would have undergone MeHg photochemical degradation to yield the observed Δ^{199}Hg shifts. Similarly,

experimental data for isotopic fractionation of Hg(II) during photoreduction in the presence of 1.2 mg/L DOC was used to estimate the proportion of Hg(II) remaining in filtered surface waters that had been subjected to photodegradation prior to incorporation in the water column (Zheng & Hintelmann, 2009). This calculation yields an estimate that the Hg mass measured in the filtered surface waters represents 74% to 85% of the Hg mass that would have been present prior to photoreduction processes.

As %MeHg (percent of THg present as MeHg) values for filtered surface waters of these watersheds are typically <10%, insufficient MeHg would be available to undergo photodegradation to produce the magnitude of MIF signatures observed, supporting the hypothesis that Hg(II) photoreduction processes are contributing to the observed MIF signatures. Additionally, the calculated proportion of MeHg in 2015 surface waters is lower than the calculated degree of photodegradation for the estimated bioavailable MeHg endmember in both the Yuba R. (2013: 24% photodegraded; 2014: 35% photodegraded) and Cache Cr. (2013: 17% photodegraded; 2014: 31% photodegraded). This evidence suggests that the bioavailable MeHg pool present in surface waters is not exclusively contributing to MIF shifts (Donovan et al., 2016a; Donovan et al., 2016b). The lesser extent of photodegradation calculated for 2015 filtered surface water may be related to a number of factors, including differences in water quality parameters (e.g. increased turbidity, increased water depth) that would result in net decreases of photoreduction, or mixing with colloidal-IHg with near-zero Δ^{199}Hg values from sediment or suspended particulate sources, resulting in a measured Δ^{199}Hg value with a smaller magnitude, thereby biasing our calculated extent of photodegradation to artificially low values.

The amount of photoreduced Hg(0) that would need to be retained in the particulate phase of the Yuba R. can be estimated using a simple mixing model calculation. Using the

400 average Δ^{199}Hg value for Yuba R. sediments (0.04‰) and the average Δ^{199}Hg value for
401 photoreduced Hg(0) (-3.88‰) from the Hg(II)-DOM photoreduction experiments conducted by
402 Zheng and Hintelmann (2009), the calculation predicts that to obtain the average Δ^{199}Hg value
403 observed for Yuba R. suspended particulates (-0.21‰) only 7% of the total Hg present in the
404 particulates needs to be retained Hg(0). With only 7% of the Hg present in the suspended
405 particulates (~10 to 20 ng/L) this is a much greater mass of Hg than is found in any of the filter-
406 passing Hg pools in the Yuba R., so this calculation may not accurately account for a factors
407 such as photoreduction of suspended particulate material as well as a potentially greater
408 magnitude of MIF shifts associated with MeHg-DOM photoreduction rather than exclusively
409 Hg(II)-DOM photoreduction.

410 **3.3 Sources of Hg to the Surface Waters of the Yuba R. and Cache Cr. Watersheds**

411 **3.3.1 Variations in the Isotopic Composition of Filtered Surface Waters and Suspended**
412 **Particulates**

413 Both MeHg and Hg(II) photoreduction processes impart δ^{202}Hg shifts, so surface water
414 Hg pools should have distinct isotopic compositions from the source Hg pools as the result of
415 these processes. For samples collected from the Yuba R., filtered surface water samples and
416 suspended particulates do have significantly different average Δ^{199}Hg values [Unpaired t-Test
417 with equal variance, n_1=6, n_2=4, T=5.333, p=0.001], but do not have significantly different
418 δ^{202}Hg values [Unpaired t-Test with equal variance, n_1=6, n_2=4, T=0.035, p=0.936], despite the
419 much greater variation in isotopic composition observed in suspended particulates.

420 For the Yuba R. watershed surface waters, no clear trends are observed between THg
421 concentration and either δ^{202}Hg values or Δ^{199}Hg values. The partition coefficients ($\log(k_D)$)
422 remain essentially constant throughout the sampling reach (5.62 to 5.72), suggesting that Hg

partitioning between the particulate phases and filter-passing phases is similar throughout the study reach, and that Hg inputs from sediment resuspension of bed/bank sediment are similar at each sampling location. Additionally, there are no clear trends between isotopic composition and sampling distance downstream. Furthermore, all samples were collected under the same hydrologic flow regime, so there does not appear to be a temporal bias that could affect Hg partitioning.

The lack of correlation between either sample location or THg concentration and the Hg isotopic composition within surface waters suggests that the Hg isotopic composition within the Yuba R. surface waters is not controlled by isotopic end-member mixing or site-specific fractionation processes at any given sampling location. Neither the filtered surface waters nor suspended particulate fractions have average δ^{202}Hg values that are significantly different from the average δ^{202}Hg values observed in river bank and terrace sediments in the Yuba R. (δ^{202}Hg = -0.38 ± 0.42 ‰ [1SD]) (Donovan et al., 2016a). The similar ranges and average δ^{202}Hg values of surface water fractions and sediments support the interpretation that river bank and terrace sediments are the main source of Hg to the surface water in the Yuba R. However, the differences in average Δ^{199}Hg values in these three sample types imply that photodegradation fractionation processes result in odd-MIF anomalies in the surface waters, but not in the bank and terrace sediments.

In Cache Cr., filtered surface water samples and suspended particulates have average δ^{202}Hg values that differ by 0.44‰, but the Hg isotopic composition of these two Hg pools is not significantly different [Unpaired t-Test with equal variance, n_1=7, n_2=2, T=2.012, p=0.084]. While not statistically significant, this pattern of positive δ^{202}Hg shifts is consistent with fractionation due to photoreduction processes. Similar to the Yuba R., the two sample types do

446 have significantly different average Δ^{199}Hg values [Unpaired t-Test with equal variance, n_1=7,
447 n_2=2, T=3.321, p=0.013]. No clear trends between THg concentration and either δ^{202}Hg values or
448 Δ^{199}Hg values are observed in the Cache Cr. surface waters. THg concentrations for both filtered
449 surface water and suspended particulates increase with distance downstream, but this increase is
450 not reflected in clear trends in Hg isotopic composition [Table 1]. Hg partition coefficients are
451 generally lower in Cache Cr. and they increase with distance downstream ($\log(k_D)$ = 5.18 to
452 5.44), which may be indicative of increasing inputs of sediment-sourced Hg in the particulate
453 phase. The riverbed and terrace sediments in Cache Cr. had a more positive average δ^{202}Hg value
454 (δ^{202}Hg = -0.84 ± 0.49‰ [1SD]) than was observed in suspended particulates, but this difference
455 was not significant [Unpaired t-Test with equal variance, n_1=7, n_2=14, T=1.933, p=0.068]
456 (Donovan et al. 2016b). Overall, there are no clear patterns in δ^{202}Hg values for Hg in surface
457 water pools in either the Yuba R. or Cache Cr. In other words, there is no good support for the
458 hypothesis that photoreduction processes exhibit a control on the isotopic compositions of
459 surface water Hg in these systems, while Δ^{199}Hg values for these same fractions do provide
460 evidence for this hypothesis. Significant heterogeneity in sediment isotopic composition between
461 sampling sites is likely contributing to this apparent decoupling between MDF and MIF
462 signatures in the surface water Hg pools.

463 **3.3.2 Influence of Sediment Hg on Surface Water Hg Isotopic Composition**

464 The relationship between filtered surface water, associated suspended particulates, and
465 bed or bank sediment samples collected at the same location (subsequently referred to as
466 "paired" samples) is shown in Figure 3. No consistent patterns are observable in the relationship
467 between δ^{202}Hg values for paired sample types from the same sampling location. Comparing
468 sediments to suspended particulates, both positive and negative δ^{202}Hg shifts (+0.75‰ to -

469 0.82‰) are observed for paired samples. Filtered surface waters also show both positive and
470 negative δ^{202}Hg shifts (+0.30‰ to -0.56‰) compared to paired sediments.
471 The apparent decoupling between the isotopic composition of Hg in paired sediments and
472 surface water compartments could be due to a number of factors. Surface water Hg fractions
473 could represent the influence of Hg incorporated at upstream locations and transported
474 downstream. Both Cache Cr. and Yuba R. sediments displayed relatively large ranges in δ^{202}Hg
475 values (Cache Cr.: -1.69‰ to -0.11‰; Yuba R.: -0.95‰ to 0.71‰). Transport of sediment-
476 bound Hg with a differing isotopic composition from upstream locations could account for the
477 δ^{202}Hg shifts observed between sediments at a specific location and suspended particulates. Our
478 sampling campaign was not conducted with sufficient spatial resolution to capture reach-scale
479 heterogeneity in Hg isotopic composition, and there may be significantly more variation than
480 previously documented.
481 As has been demonstrated in the limited number of studies that have investigated the
482 isotopic composition of suspended particulate phase Hg in surface waters (Foucher et al., 2013;
483 Washburn et al., 2017; Jiskra et al., 2017; Washburn et al., 2018b; Demers et al., 2018; Baptista-
484 Salazar et al., 2018), there are a number of processes, such as sorption to mineral phases or
485 aqueous photochemical reduction of Hg, that can produce significant δ^{202}Hg shifts in this Hg
486 pool relative to a Hg source (Jiskra et al., 2012; Bergquist and Blum, 2007). A number of
487 sampling site-specific factors, such as turbidity, solar insolation, and biotic activity, could all
488 alter the degree to which certain fractionation processes were occurring at any site. As both
489 positive and negative isotopic shifts were observed from sediment to suspended particulates, no
490 single fractionation processes can be invoked to explain the variation in surface water data.
491 Δ^{199}Hg values of co-located "paired" samples of filtered surface water, suspended

492 particulates and stream sediment exhibit similar behavior at each sample site. All suspended
493 particulate samples had lower Δ^{199}Hg values compared to sediments, except for the Rumsey site,
494 where the suspended particulates are within uncertainty of the sediment value (suspended
495 particulates Δ^{199}Hg = 0.12‰, sediment Δ^{199}Hg = 0.09‰). All filtered surface water samples
496 showed more positive Δ^{199}Hg values than co-located sediment samples. Unlike the lack of
497 pattern in δ^{202}Hg values for paired samples, the consistent pattern observed for Δ^{199}Hg values is
498 suggestive of a single fractionation process controlling the odd-MIF composition of the surface
499 water samples, namely Hg photodegradation as discussed in depth in Section 3.2.
500 **3.3.3 Influence of Hydrothermal Activity on the Isotopic Composition of Hg in Sulfur**
501 **Creek**
502 The isotopic composition of these samples is likely impacted by the hydrothermal activity
503 and hot springs (Wilbur Springs) in the headwaters of this stream. The isotopic composition of
504 the surface waters we measured in Sulfur Creek are distinctly different than those reported in
505 Smith et al., 2008 for hydrothermal spring precipitates collected from Wilbur Springs (δ^{202}Hg = -
506 0.95‰, Δ^{201}Hg = 0.11‰), but they are within the range of δ^{202}Hg values for other hydrothermal
507 spring precipitates from the same region of the Coast Range hydrothermal complex (δ^{202}Hg = -
508 0.95‰ to -3.42‰, Δ^{201}Hg = 0.11‰ to 0.32‰). The relatively more negative δ^{202}Hg values
509 observed in Sulfur Creek compared to the Wilbur Springs hydrothermal precipitates could be the
510 result of a temporally variable hydrothermal Hg source to the hot springs, or the result of
511 fractionation related to the precipitation of Hg from the hydrothermal fluid as suggested by
512 Smith et al. (2008). The large magnitude odd-MIF signatures observed in the surface waters of
513 Sulfur Cr. are likely a result of both the elevated above regional background odd MIF signatures
514 of the hydrothermally-derived Hg due to hydrothermal processing, and subsequent

photoreduction processes occurring after the hydrothermally-derived Hg reaches the surface environment (discussed in Section 3.2).

To determine the influence of Sulfur Creek on the Hg isotopic composition of Bear Creek, surface water samples were obtained both above and below the confluence of Sulfur Cr. with Bear Cr. Below the confluence (Bear Cr. at Holston Chimney Canyon), the filtered surface water and suspended particulate fractions both exhibited elevated THg concentrations compared to measurements taken above the confluence, providing evidence for an influx of Hg from Sulfur Cr. into Bear Cr. The δ^{202}Hg value for suspended particulates collected at Holston Chimney Canyon (δ^{202}Hg = -1.03‰) was plotted versus 1/THg to evaluate mixing relationships between particulates from Sulfur Cr. (δ^{202}Hg = -2.89‰) and Bear Cr. above the confluence with Sulfur Cr. (δ^{202}Hg = -1.39‰). The samples do not exhibit a significant a linear trend [linear least squares regression, slope = 2389.7 ± 1925.2, p = 0.37], as particulates from Holston Chimney Canyon have a much less negative δ^{202}Hg value that cannot be explained due to inputs of Hg from Sulfur Cr. The lack of a linear relationship between the 1/THg concentration data and the isotope data is likely due to the occurrence of fractionation of Hg originating from Sulfur Cr. once it has entered Bear Cr. Although the Δ^{199}Hg value observed in particulates at Holston Chimney Canyon (Δ^{199}Hg = 0.53‰) is intermediate between Sulfur Cr. (Δ^{199}Hg = 0.70‰) and Bear Cr. above the confluence (Δ^{199}Hg = 0.20‰), this value is likely affected by fractionation during photoreduction and other MIF-inducing processes, and does not directly provide evidence for source mixing in Bear Cr.

3.3.4 Δ^{204}Hg and Δ^{200}Hg Signatures of Surface Waters

None of the filtered surface water samples in the Yuba R. or Cache Cr. has even-MIF signatures of significant magnitude (Figure S1). Of the suspended particulate samples, only 5

samples have Δ^{204}Hg values that are distinguishable from 0.00‰ based on analytical uncertainty (±0.20‰), and only two of these samples (Simpson Bridge site on the Yuba R., Δ^{204}Hg = -0.29‰, Δ^{200}Hg = -0.01‰; Bear Cr. above Sulfur Cr., Δ^{204}Hg = -0.40‰, Δ^{200}Hg = 0.04‰ [Table 1]) exhibit negative Δ^{204}Hg values that would be consistent with Hg derived from un-impacted North American atmospheric precipitation, but these suspended particulates do not exhibit Δ^{200}Hg values that are different from 0.00‰ (Gratz et al., 2010; Chen et al., 2012; Demers et al., 2013; Donovan et al., 2013; Cai and Chen, 2015). Two suspended particulate samples (Dantoni and Parks Bar sites on the Yuba R.) have even MIF signatures consistent with observations of un-impacted atmospheric total gaseous Hg (positive Δ^{204}Hg values, negative Δ^{200}Hg values) (Gratz et al., 2010; Sherman et al., 2010; Demers et al., 2013; Demers et al., 2015; Fu et al., 2016; Yu et al., 2016). These two samples were run at the lowest (0.35 ng/g) and next to lowest (0.5 ng/g) run solution concentrations, and UM-Almadén run concurrently at these concentrations yielded much greater analytical uncertainty (0.35 ng/g run solution: Δ^{204}Hg±0.56‰; Δ^{200}Hg±0.28‰, n=5), suggesting that the anomalously large magnitude even-MIF signatures observed in these two samples are unlikely to represent natural processes or sources affecting the suspended particulate load at these two locations. Based on the lack of significant even-MIF signatures in the surface water samples, atmospherically-derived Hg is unlikely to be a significant contributor to the total Hg load in surface waters of the studied watersheds. The even-MIF signatures of these surface water samples provide additional evidence that the predominant Hg source within these systems is related to mining-derived activities rather than atmospheric deposition, in agreement with a previous study that estimated the contributions of atmospheric Hg deposition to these watersheds (Domagalski et al., 2016).

3.4 Comparison of Surface Water Hg Isotopic Composition to Biota within the Yuba R.

and Cache Cr. Watersheds

Utilizing Hg stable isotopes to identify the transformations that lead to a bioavailable pool of Hg within surface water compartments of fluvial systems was a motivation for conducting this work. For both the Yuba R. and Cache Cr. systems, filtered surface water Hg pools have very similar δ^{202}Hg, Δ^{201}Hg, and Δ^{199}Hg values as the lower trophic position invertebrates reported in Donovan et al., 2016a and Donovan et al., 2016b (Fig. 1, Fig. 2). The concordant isotopic signatures in low trophic position invertebrates and filtered surface waters is suggestive that the Hg reservoirs in both of these sample types have undergone similar environmental processing, imparting similar degrees of isotopic fractionation. It is important to note that for low trophic position biota, a significant portion of the Hg present within their tissues is inorganic Hg (Hg(II) complexes), and that this inorganic Hg is thought to not bioaccumulate to as significant a degree as MeHg. Previous studies have suggested that the MIF signatures of Hg incorporated by biota are unlikely to be fractionated by internal processes (Perrot et al., 2012; Kwon et al., 2013). The lack of MIF fractionation within biota suggests that both Hg(II) and MeHg affected by photoreduction within surface water prior to incorporation within biota would impart elevated odd-MIF signatures to those biota.

For both watersheds, the vast majority of biota have Δ^{199}Hg/Δ^{201}Hg ratio values that fall within uncertainty of the slope predicted for surface water samples collected in this study (1.52±0.24) (Fig. S1), evidence that the Hg(II) and MeHg within these organisms is being affected by the same photoreduction processes suggested to be producing the MIF within the surface water Hg pools. In other words, filter-passing MeHg in the water column could be to a significant source of MeHg to food webs in these rivers systems. Furthermore, when the Δ^{199}Hg/Δ^{201}Hg slopes are evaluated for specific sampling sites at which biota, sediment, and

584 surface water samples have all been collected, the site-specific slopes are all within error of the
585 overall $\Delta^{199}Hg/\Delta^{201}Hg$ slopes for surface waters in each river (Figure S4). Although the
586 sediment, biota, and surface water samples were collected during different years (they were,
587 however, collected during the same season), it appears that the processes controlling MIF
588 fractionation within these two river systems are relatively constant temporally and spatially
589 within the rivers.
590 In the Yuba R., the range in filtered surface water isotopic composition ($\delta^{202}Hg$ = -0.82‰
591 to -0.50‰, $\Delta^{199}Hg$ = 0.37‰ to 0.62‰) is similar to a subset of invertebrate organisms with
592 between 37%-143% %MeHg ($\delta^{202}Hg$ = -0.76‰ to -0.47‰, $\Delta^{199}Hg$ = 0.27‰ to 0.62‰), and
593 much more positive $\Delta^{199}Hg$ values than filamentous algae samples with 2-17% %MeHg ($\delta^{202}Hg$
594 = -0.82‰ to -0.61‰, $\Delta^{199}Hg$ = 0.06‰ to 0.16‰) (Donovan et al., 2016a). Similarly, in Cache
595 Cr. the range in filtered surface water isotopic composition ($\delta^{202}Hg$ = -0.84‰ to -0.73‰, $\Delta^{199}Hg$
596 = 0.58‰ to 0.64‰, excluding the Sulfur Cr. FSW samples) is within the range exhibited by a
597 subset of invertebrate organisms with between 38%-115% %MeHg ($\delta^{202}Hg$ = -1.23‰ to -0.69‰,
598 $\Delta^{199}Hg$ = 0.51‰ to 0.69‰) (Donovan et al., 2016b). Interestingly, filamentous algae samples
599 from Cache Cr. exhibited a much greater range in $\Delta^{199}Hg$ values ($\Delta^{199}Hg$ = 0.37‰ to 1.00‰,
600 $\delta^{202}Hg$ = -1.15‰ to -0.34‰) and %MeHg (20%-60%), which Donovan et al (2016a) attributed
601 to multiple, isotopically distinct pools of IHg and MeHg in the Cache Cr. system. The large
602 range in filtered surface water isotopic composition observed within the headwaters of Cache
603 Cr., including Sulfur Cr., is consistent with the interpretation that there could be a number of
604 isotopically distinct IHg pools that could undergo methylation and incorporation into low trophic
605 position biota. Such an interpretation would necessitate that MeHg photoreduction was occurring
606 predominantly while MeHg was associated with small particles or dissolved in surface waters

prior to incorporation into the food chain. At present, there is insufficient supporting data to confidently make such a claim, and future studies are needed to understand this complex portion of the Hg cycle. Future studies should focus on the relationship between low trophic position biota and filtered surface water Hg isotopic composition, particularly as they fluctuate temporally and with hydrologic conditions.

In both Cache Cr. and the Yuba R., negative δ^{202}Hg shifts were observed between the estimated IHg source and the estimated pre-photodegraded MeHg source (Donovan et al., 2016a; Donovan et al., 2016b). One hypothesis suggested for this negative δ^{202}Hg offset was that *in situ* methylation of Hg within sediments, followed by MeHg advection into the water column and transport downstream by flowing water, would produce a local bioavailable MeHg pool that had undergone minimal biotic MeHg degradation, thus exhibiting more negative net biotic fractionation shift (Donovan et al., 2016a; Donovan et al., 2016b). The isotopic compositions of Hg within the surface waters of Cache Cr. and Yuba R. support this hypothesis, as evidenced by the overlapping isotopic composition with biota. The reservoir of MeHg that is bioavailable and being bioaccumulated within the biota of these fluvial systems is isotopically similar to the Hg reservoir within surface waters. The temporal differences in the isotopic composition of the estimated MeHg end-member observed in the previous studies of these river systems, combined with the lack of temporally concurrent biota data to accompany the 2015 surface water samples prevents us from unequivocally concluding that surface waters are the source of MeHg to the aquatic biota in these river systems. However, the concordant isotopic compositions of Hg in filtered surface waters and low trophic position biota is highly suggestive that the MeHg and Hg(II) in the two compartments is from the same source, and accumulation of surface water MeHg by biota is consistent with the isotopic data.

3.5 Future Implications and Conclusions

We applied stable Hg isotope measurement techniques to surface water samples from two California river systems affected by extensive legacy mining-related Hg contamination in order to better elucidate the biogeochemical cycling of Hg on the path to bioavailability. Isotopic evidence, particularly odd-MIF signatures, indicate that Hg photoreduction processes are occurring within Yuba R. and Cache Cr. surface waters to a significant degree. Within the Yuba R., the isotopic composition of suspended particulate phases suggests retention of the reduced product of MeHg and Hg(II) photoreduction may be occurring. Importantly, the similar isotopic compositions of filtered surface waters and low trophic position biota within these watersheds indicates that the reservoir of Hg within the biota of these California rivers is similar to the filter-passing fraction of Hg in surface waters. Future studies should utilize the Hg preconcentration methods such as the one employed here to analyze other low Hg concentration freshwaters to expand the understanding of the biogeochemical cycle of Hg in aquatic ecosystems that had previously been analytically difficult or unfeasible.

Acknowledgements

We thank Marcus Johnson for his patient assistance and guidance in operating the CV-MC-ICP-MS at the University of Michigan, as well as his assistance in calculating regression statistics. We thank Bridget Bergquist for allowing us to analyze samples at the University of Toronto and Priyanka Chandan for her assistance in operating the CV-MC-ICP-MS at the University of Toronto. We would also like to thank Zach Jaco and Tyler Nakamura for their assistance with field sampling. This work was partially funded from a University of Michigan Department of Earth and Environmental Sciences Scott Turner Award to S.J.W. We also

652 acknowledge financial support from the National Science Foundation: EAR-1225630 (to J.D.B.)
653 and EAR-1226741 (to M.B.S.).

654 **Corresponding Author**

655 * Spencer J. Washburn
656 Smithsonian Environmental Research Center
657 647 Contees Wharf Road
658 Edgewater, MD 21037 USA
659 Email: washburns@si.edu
660 Phone: 443-482-2389
661

662 **Supporting Information**

663 The Supporting Information includes an unabridged methods section, and six figures, and
664 one table.

References

(1) Alpers, C. N.; Hunerlach, M. P.; May, J. T.; Hothem, R. L. Mercury Contamination from Historical Gold Mining in California. Publications of the U.S. Geologic Survey. **2005**, *61*.

(2) Alpers, C. N.; Hunerlach, M. P.; May, J. T.; Hothem, R. L.; Taylor, H. E.; Antweiler, R. C.; De Wild, J. F.; Lawler, D. a. Geochemical Characterization of Water, Sediment, and Biota Affected by Mercury Contamination and Acidic Drainage from Historical Gold Mining, Greenhorn Creek, Nevada County, California, 1999-2001. Scientific Investigative Report 2004-5251 **2004**, U.S. Geologic Survey.

(3) Baptista-Salazar, C.; Hintelmann, H.; Biester, H. Distribution of Mercury Species and Mercury Isotope Ratios in Soils and River Suspended Matter of a Mercury Mining Area. *Environ. Sci. Process. Impacts* **2018**, *00*, 1–11 DOI: 10.1039/C7EM00443E.

(4) Bergquist, B. A.; Blum, J. D. Mass-Dependent and -Independent Fractionation of Hg Isotopes by Photoreduction in Aquatic Systems. *Science* **2007**, *318* (5849), 417–420 DOI: 10.1126/science.1148050.

(5) Biswas, A.; Blum, J. D.; Bergquist, B. A.; Keeler, G. J.; Xie, Z. Natural Mercury Isotope Variation in Coal Deposits and Organic Soils. *Environ. Sci. Technol.* **2008**, *42* (22), 8303–8309 DOI: 10.1021/es801444b.

(6) Blum, J. D.; Bergquist, B. a. Reporting of Variations in the Natural Isotopic Composition of Mercury. *Anal. Bioanal. Chem.* **2007**, *388* (2), 353–359 DOI: 10.1007/s00216-007-1236-9.

(7) Blum, J. D.; Johnson, M. W. Recent Developments in Mercury Stable Isotope Analysis. *Rev. Mineral. Geochemistry* **2017**, *82* (1), 733–757 DOI: https://doi.org/10.2138/rmg.2017.82.17.

(8) Blum, J. D.; Sherman, L. S.; Johnson, M. W. Mercury Isotopes in Earth and Environmental Sciences. *Annu. Rev. Earth Planet. Sci.* **2014**, *42* (1), 249–269 DOI: 10.1146/annurev-earth-050212-124107.

(9) Böckelmann, U.; Manz, W.; Neu, T. R.; Szewzyk, U. Characterization of the Microbial Community of Lotic Organic Aggregates ('river Snow') in the Elbe River of Germany by Cultivation and Molecular Methods. *FEMS Microbiol. Ecol.* **2000**, *33* (2), 157–170 DOI: 10.1016/S0168-6496(00)00056-8.

(10) Bouse, R. M.; Fuller, C. C.; Luoma, S.; Hornberger, M. I.; Jaffe, B. E.; Smith, R. E. Mercury-Contaminated Hydraulic Mining Debris in San Francisco Bay. *San Fr. Estuary Watershed Sci.* **2010**, *8* (1).

(11) Cai, H.; Chen, J. Mass-Independent Fractionation of Even Mercury Isotopes. *Sci. Bull.* **2015**, *61* (January), 116–124 DOI: 10.1007/s11434-015-0968-8.

(12) Chandan, P.; Ghosh, S.; Bergquist, B. a. Mercury Isotope Fractionation during Aqueous Photoreduction of Monomethylmercury in the Presence of Dissolved Organic Matter. *Environ. Sci. Technol.* **2015**, *49* (1), 259–267 DOI: 10.1021/es5034553.

(13) Chen, J. Bin; Hintelmann, H.; Feng, X. Bin; Dimock, B. Unusual Fractionation of Both Odd and Even Mercury Isotopes in Precipitation from Peterborough, ON, Canada. *Geochim. Cosmochim. Acta* **2012**, *90*, 33–46 DOI: 10.1016/j.gca.2012.05.005.

(14) Chow, A. T.; Dahlgren, R. A.; Harrison, J. A. Watershed Sources of Disinfection Byproduct Precursors in the Sacramento and San Joaquin Rivers, California. *Environ. Sci. Technol.* **2007**, *41* (22), 7645–7652 DOI: 10.1021/es070621t.

(15) Demers, J. D.; Blum, J. D.; Brooks, S.; Donovan, P. M.; Riscassi, A.; Miller, C. L.; Zheng, W.; Gu, B. Hg Isotopes Reveal In-Stream Processing and Legacy Inputs in East Fork Poplar Creek, Oak Ridge, Tennessee, USA. *Environ. Sci. Process. Impacts* **2018** DOI: 10.1039/C7EM00538E.

(16) Demers, J. D.; Blum, J. D.; Zak, D. R. Mercury Isotopes in a Forested Ecosystem: Implications for Air-Surface Exchange Dynamics and the Global Mercury Cycle. *Global Biogeochem. Cycles* **2013**, *27*, n/a-n/a DOI: 10.1002/gbc.20021.

(17) Demers, J. D.; Sherman, L. S.; Blum, J. D.; Marsik, F. J.; Dvonch, J. T. Coupling Atmospheric Mercury Isotope Ratios and Meteorology to Identify Sources of Mercury Impacting a Coastal Urban-Industrial Region near Pensacola, Florida, USA. *Global Biogeochem. Cycles* **2015**, *29* (10), 1689–1705 DOI: 10.1002/2015GB005146.

(18) Domagalski, J. L.; Slotton, D. G.; Alpers, C. N.; Suchanek, T. H.; Churchill, R.; Bloom, N.; Ayers, S. M.; Clinkenbeard, J. Summary and Synthesis of Mercury Studies in the Cache Creek Watershed, California, 2000-2001. Water-Resources Investigative Report 03-4335. **2004**, U.S. Geologic Survey.

(19) Domagalski, J. L. Mercury and Methylmercury in Water and Sediment of the Sacramento River Basin, California. *Appl. Geochemistry* **2001**, *16*, 1677–1691.

(20) Domagalski, J. L.; Alpers, C. N.; Slotton, D. G.; Suchanek, T. H.; Ayers, S. M. Mercury and Methylmercury Concentrations and Loads in the Cache Creek Watershed, California. *Sci. Total Environ.* **2004**, *327* (1–3), 215–237 DOI: 10.1016/j.scitotenv.2004.01.013.

(21) Donovan, P. M.; Blum, J. D.; Singer, M. B.; Marvin-DiPasquale, M.; Tsui, M. T. K. Methylmercury Degradation and Exposure Pathways in Streams and Wetlands Impacted by Historical Mining. *Sci. Total Environ.* **2016** DOI: 10.1016/j.scitotenv.2016.04.139.

(22) Donovan, P. M.; Blum, J. D.; Singer, M. B.; Marvin-DiPasquale, M.; Tsui, M. T. K. Isotopic Composition of Inorganic Mercury and Methylmercury Downstream of a Historical Gold Mining Region. *Environ. Sci. Technol.* **2016**, acs.est.5b04413 DOI: 10.1021/acs.est.5b04413.

(23) Donovan, P. M.; Blum, J. D.; Yee, D.; Gehrke, G. E.; Singer, M. B. An Isotopic Record of Mercury in San Francisco Bay Sediment. *Chem. Geol.* **2013** DOI: 10.1016/j.chemgeo.2013.04.017.

(24) Eagles-Smith, C. A.; Ackerman, J. T.; De La Cruz, S. E. W.; Takekawa, J. Y. Mercury Bioaccumulation and Risk to Three Waterbird Foraging Guilds Is Influenced by Foraging Ecology and Breeding Stage. *Environ. Pollut.* **2009**, *157* (7), 1993–2002 DOI: 10.1016/j.envpol.2009.03.030.

(25) Estrade, N.; Carignan, J.; Donard, O. F. X. Tracing and Quantifying Anthropogenic Mercury Sources in Soils of Northern France Using Isotopic Signatures. *Environ. Sci. Technol.* **2011**, *45* (4), 1235–1242 DOI: 10.1021/es1026823.

(26) Fleck, J. A.; Alpers, C. N.; Marvin-DiPasquale, M.; Hothem, R. L.; Wright, S. A.; Ellett, K.; Beaulieu, E.; Agee, J. L.; Kakouros, E.; Kieu, L. H.; Eberl, D. D.; Blum, A. E.; May, J. T. The Effects of Sediment and Mercury Mobilization in the South Yuba River and Humbug Creek Confluence Area, Nevada County, California: Concentrations, Speciation and Environmental Fate-Part 1: Field Characterization. Open-File Rep. 2010-1325A**. 2011**, U.S. Geologic Survey.

(27) Foucher, D.; Hintelmann, H.; Al, T. a.; MacQuarrie, K. T. Mercury Isotope Fractionation in Waters and Sediments of the Murray Brook Mine Watershed (New Brunswick, Canada): Tracing Mercury Contamination and Transformation. *Chem. Geol.* **2013**, *336*, 87–95 DOI: 10.1016/j.chemgeo.2012.04.014.

(28) Fu, X.; Marusczak, N.; Wang, X.; Gheusi, F.; Sonke, J. E. Isotopic Composition of Gaseous Elemental Mercury in the Free Troposphere of the Pic Du Midi Observatory, France. *Environ. Sci. Technol.* **2016**, *50* (11), 5641–5650 DOI: 10.1021/acs.est.6b00033.

(29) Ghoshal, S.; James, L. A.; Singer, M. B.; Aalto, R. Channel and Floodplain Change Analysis over a 100-Year Period: Lower Yuba River, California. *Remote Sens.* **2010**, *2* (7), 1797–1825 DOI: 10.3390/rs2071797.

(30) Gratz, L. E.; Keeler, G. J.; Blum, J. D.; Sherman, L. S. Isotopic Composition and Fractionation of Mercury in Great Lakes Precipitation and Ambient Air. *Environ. Sci. Technol.* **2010**, *44* (20), 7764–7770 DOI: 10.1021/es100383w.

(31) Greenfield, B. K.; Jahn, A. Mercury in San Francisco Bay Forage Fish. *Environ. Pollut.* **2010**, *158* (8), 2716–2724 DOI: 10.1016/j.envpol.2010.04.010.

(32) Gu, B.; Bian, Y.; Miller, C. L.; Dong, W.; Jiang, X.; Liang, L. Mercury Reduction and Oxidation by Reduced Natural Organic Matter in Anoxic Environments. *Environ. Sci. Technol.* **2012**, *46* (1), 292–299 DOI: 10.1021/es203402p.

(33) Higson, J. L.; Singer, M. B. The Impact of the Streamflow Hydrograph on Sediment Supply from Terrace Erosion. *Geomorphology* **2015**, *248*, 475–488 DOI: 10.1016/j.geomorph.2015.07.037.

(34) Hothem, R. L.; Bergen, D. R.; Bauer, M. L.; Crayon, J. J.; Meckstroth, A. M. Mercury and Trace Elements in Crayfish from Northern California. *Bull. Environ. Contam. Toxicol.* **2007**, *79* (6), 628–632 DOI: 10.1007/s00128-007-9304-6.

(35) Hothem, R. L.; Jennings, M. R.; Crayon, J. J. Mercury Contamination in Three Species of Anuran Amphibians from the Cache Creek Watershed, California, USA. *Environ. Monit. Assess.* **2010**, *163* (1–4), 433–448 DOI: 10.1007/s10661-009-0847-3.

(36) Hothem, R. L.; Trejo, B. S.; Bauer, M. L.; Crayon, J. J. Cliff Swallows Petrochelidon Pyrrhonota as Bioindicators of Environmental Mercury, Cache Creek Watershed, California. *Arch. Environ. Contam. Toxicol.* **2008**, *55* (1), 111–121 DOI: 10.1007/s00244-007-9082-5.

(37) Hunerlach, M. P.; Alpers, C. N.; Marvin-Dipasquale, M.; Taylor, H. E.; De Wild, J. F. Geochemistry of Mercury and Other Trace Elements in Fluvial Tailings Upstream of Daguerre Point Dam, Yuba River, California, August 2001. Scientific Investigative Report 2004-5165. **2004**, U.S. Geologic Survey.

(38) Hurley, J. P.; Cowell, S. E.; Shafer, M. M.; Hughes, P. E. Partitioning and Transport of Total and Methyl Mercury in the Lower Fox River, Wisconsin. *Environ. Sci. Technol.* **1998**, *32* (10), 1424–1432 DOI: 10.1021/es970685b.

(39) James, L. A.; Singer, M. B.; Ghoshal, S.; Megison, M. Historical Channel Changes in the Lower Yuba and Feather Rivers, California: Long-Term Effects of Contrasting River-Management Strategies. *Spec. Pap. Geol. Soc. Am.* **2009**, *451* (04), 57–61 DOI: 10.1130/2009.2451(04).

(40) Jiskra, M.; Wiederhold, J. G.; Bourdon, B.; Kretzschmar, R. Solution Speciation Controls Mercury Isotope Fractionation of Hg(II) Sorption to Goethite. *Environ. Sci. Technol.* **2012**, *46* (12), 6654–6662 DOI: 10.1021/es3008112.

(41) Jiskra, M.; Wiederhold, J. G.; Skyllberg, U.; Kronberg, R. M.; Hajdas, I.; Kretzschmar, R. Mercury Deposition and Re-Emission Pathways in Boreal Forest Soils Investigated with Hg Isotope Signatures. *Environ. Sci. Technol.* **2015**, *49* (12), 7188–7196 DOI: 10.1021/acs.est.5b00742.

(42) Jiskra, M.; Wiederhold, J.; Skyllberg, U.; Kronberg, R.-M.; Kretzschmar, R. Source Tracing of Natural Organic Matter Bound Mercury in Boreal Forest Runoff with Mercury Stable Isotopes. *Environ. Sci. Process. Impacts* **2017**, *00*, 1–14 DOI: 10.1039/C7EM00245A.

(43) Kritee, K.; Barkay, T.; Blum, J. D. Mass Dependent Stable Isotope Fractionation of Mercury during Mer Mediated Microbial Degradation of Monomethylmercury. *Geochim. Cosmochim. Acta* **2009**, *73* (5), 1285–1296 DOI: 10.1016/j.gca.2008.11.038.

(44) Kwon, S. Y.; Blum, J. D.; Nadelhoffer, K. J.; Timothy Dvonch, J.; Tsui, M. T. K. Isotopic Study of Mercury Sources and Transfer between a Freshwater Lake and Adjacent Forest Food Web. Sci. Total Environ. 2015, 532, 220–229 DOI: 10.1016/j.scitotenv.2015.06.012.

(45) Kwon, S. Y.; Blum, J. D.; Nadelhoffer, K. J.; Timothy Dvonch, J.; Tsui, M. T. K. Isotopic Study of Mercury Sources and Transfer between a Freshwater Lake and Adjacent Forest Food Web. *Sci. Total Environ.* **2015**, *532*, 220–229 DOI: 10.1016/j.scitotenv.2015.06.012.

(46) Lepak, R. F.; Janssen, S. E.; Yin, R.; Krabbenhoft, D. P.; Ogorek, J. M.; DeWild, J. F.; Tate, M. T.; Holsen, T. M.; Hurley, J. P. Factors Affecting Mercury Stable Isotopic Distribution in Piscivorous Fish of the Laurentian Great Lakes. *Environ. Sci. Technol.* **2018**, acs.est.7b06120 DOI: 10.1021/acs.est.7b06120.

(47) Marvin-DiPasquale, M.; Agee, J.; Bouse, R.; Jaffe, B. Microbial Cycling of Mercury in Contaminated Pelagic and Wetland Sediments of San Pablo Bay, California. *Environ. Geol.* **2003**, *43* (3), 260–267 DOI: 10.1007/s00254-002-0623-y.

(48) Marvin-DiPasquale, M.; Alpers, C. N.; Fleck, J. A. Mercury, Methylmercury, and Other Constituents in Sediment and Water from Seasonal and Permanent Wetlands in the Cache Creek Settling Basin and Yolo Bypass, Yolo County, California, 2005−06. Open File Rep. 2009-1182. **2009**, U.S. Geologic Survey.

(49) Marvin-DiPasquale, M.; Agee, J. L.; Kakouros, E.; Kieu, L. H.; Fleck, J. A.; Alpers, C. N. The Effects of Sediment and Mercury Mobilization in the South Yuba River and Humbug Creek Confluence Area, Nevada County, California: Concentrations, Speciation and Environmental Fate-Part 2: Laboratory Experiments. Open-File Rep. 2010-1325-B. **2011**, U.S. Geologic Survey.

(50) May, J. T.; Hothem, R. L.; Alpers, C. N.; Law, M. A. Mercury Bioaccumulation in Fish in a Region Affected by Historic Gold Mining : The South Yuba River , Deer Creek , and Bear River Watersheds , California , 1999. Open File Report 00-367. **2000**, U.S. Geologic Survey.

(51) Nakamura, T. K.; Singer, M. B.; Gabet, E. J. Remains of the 19 Th Century : Deep Storage of Contaminated Hydraulic Mining Sediment along the Lower Yuba River , California. *Elem. Sci. Anthr.* **2018**, *6* (70) DOI: https://doi.org/10.1525/elementa.333.

(52) Ortiz, V. L.; Mason, R. P.; Evan Ward, J. An Examination of the Factors Influencing Mercury and Methylmercury Particulate Distributions, Methylation and Demethylation Rates in Laboratory-Generated Marine Snow. *Mar. Chem.* **2015**, *177*, 753–762 DOI: 10.1016/j.marchem.2015.07.006.

(53) Perrot, V.; Pastukhov, M.V.; Epov, V.N.; Husted, S.; Donard, O.F.X.; Amouroux, D. Higher Mass-Independent Isotope Fractionation of Methylmercury in the Pelagic Food Web of Lake Baikal (Russia). *Environ. Sci. Technol.* **2012**, *46* (11), 5902–5911 DOI: 10.1021/es204572g.

(54) Rodŕiguez-Gonźalez, P.; Epov, V. N.; Bridou, R.; Tessier, E.; Guyoneaud, R.; Monperrus, M.; Amouroux, D. Species-Specific Stable Isotope Fractionation of Mercury during Hg(II) Methylation by an Anaerobic Bacteria (Desulfobulbus Propionicus) under Dark Conditions. *Environ. Sci. Technol.* **2009**, *43* (24), 9183–9188 DOI: 10.1021/es902206j.

(55) Rose, C. H.; Ghosh, S.; Blum, J. D.; Bergquist, B. A. Effects of Ultraviolet Radiation on Mercury Isotope Fractionation during Photo-Reduction for Inorganic and Organic Mercury Species. *Chem. Geol.* **2015**, *405*, 102–111 DOI: 10.1016/j.chemgeo.2015.02.025.

(56) Sherman, L. S.; Blum, J. D.; Johnson, K. P.; Keeler, G. J.; Barres, J. A.; Douglas, T. A. Mass-Independent Fractionation of Mercury Isotopes in Arctic Snow Driven by Sunlight. *Nat. Geosci* **2010**, *3* (3), 173–177.

(57) Sherman, L. S.; Blum, J. D. Mercury Stable Isotopes in Sediments and Largemouth Bass from Florida Lakes, USA. *Sci. Total Environ.* **2013**, *448*, 163–175 DOI: 10.1016/j.scitotenv.2012.09.038.

(58) Singer, M. B.; Aalto, R.; James, L. A.; Kilham, N. E.; Higson, J. L.; Ghoshal, S. Enduring Legacy of a Toxic Fan via Episodic Redistribution of California Gold Mining Debris. *Proc. Natl. Acad. Sci. U. S. A.* **2013**, *110* (46), 18436–18441 DOI: 10.1073/pnas.1302295110.

(59) Singer, M. B.; Harrison, L. R.; Donovan, P. M.; Blum, J. D.; Marvin-DiPasquale, M. Hydrologic Indicators of Hot Spots and Hot Moments of Mercury Methylation Potential along River Corridors. *Sci. Total Environ.* **2016**, *568*, 697–711 DOI: 10.1016/j.scitotenv.2016.03.005.

(60) Smith, C. N.; Kesler, S. E.; Blum, J. D.; Rytuba, J. J. Isotope Geochemistry of Mercury in Source Rocks, Mineral Deposits and Spring Deposits of the California Coast Ranges, USA. *Earth Planet. Sci. Lett.* **2008**, *269* (3–4), 398–406 DOI: 10.1016/j.epsl.2008.02.029.

(61) Springborn, M.; Singer, M. B.; Dunne, T. Sediment-Adsorbed Total Mercury Flux through Yolo Bypass, the Primary Floodway and Wetland in the Sacramento Valley, California. *Sci. Total Environ.* **2011**, *412–413*, 203–213 DOI: 10.1016/j.scitotenv.2011.10.004.

(62) Štrok, M.; Hintelmann, H.; Dimock, B. Development of Pre-Concentration Procedure for the Determination of Hg Isotope Ratios in Seawater Samples. *Anal. Chim. Acta* **2014**, *851*, 57–63 DOI: 10.1016/j.aca.2014.09.005.

(63) Stumpner, E.B., Alpers, C.N., Marvin-DiPasquale, M., Agee, J.L., Kakouros, E., Arias, M.R., Kieu, L.H., Roth, D.A., Slotton, D.G., and Fleck, J.A. Geochemical data for water, streambed sediment, and fish tissue from the Sierra Nevada Mercury Impairment Project, 2011–12. 2**018**, U.S. Geological Survey Data Series 1056, 133 p., https://doi.org/10.3133/ds1056.

(64) Suchanek, T. H.; Hothem, R. L.; Rytuba, J. J.; Yee, J. L. Mercury Assessment and Monitoring Protocol for the Bear Creek Watershed , Colusa County , California. Scientific Investigative Report 2010-5018. **2010**, U.S. Geologic Survey.

(65) Tsui, M. T. K.; Blum, J. D.; Finlay, J. C.; Balogh, S. J.; Kwon, S. Y. Photodegradation of Methylmercury in Stream Ecosystems. *Limnol. Oceanogr.* **2013**, *58* (1), 13–22 DOI: 10.4319/lo.2013.58.1.0013.

(66) US-EPA. Method 1631: Mercury in Water by Oxidation, Purge and Trap, and Cold Vapor Atomic Fluorescence Spectrometry. *EPA 821-R-96-012. US EPA, Off. Water, Washington, DC* **2002**, August, 1–46.

(67) US-EPA. Method 1669 Sampling Ambient Water for Trace Metals at EPA Water Quality Criteria Levels July 1996. *U.S. Environ. Prot. Agency Off. Water Eng. Anal. Div.* **1996**, July, 37.

(68) Ward, D. M.; Nislow, K. H.; Folt, C. L. Bioaccumulation Syndrome: Identifying Factors That Make Some Stream Food Webs Prone to Elevated Mercury Bioaccumulation. *Ann. N. Y. Acad. Sci.* **2010**, *1195*, 62–83 DOI: 10.1111/j.1749-6632.2010.05456.x.

(69) Washburn, S. J.; Blum, J. D.; Demers, J. D.; Kurz, A. Y.; Landis, R. C. Isotopic Characterization of Mercury Downstream of Historic Industrial Contamination in the South River, Virginia. *Environ. Sci. Technol.* **2017**, *51* (19), 10965–10973 DOI: 10.1021/acs.est.7b02577.

(70) Washburn, S. J.; Blum, J. D.; Johnson, M. W.; Tomes, J. M.; Carnell, P. J. Isotopic Characterization of Mercury in Natural Gas via Analysis of Mercury Removal Unit Catalysts. *ACS Earth Sp. Chem.* **2018**, acsearthspacechem.7b00118 DOI: 10.1021/acsearthspacechem.7b00118.

(71) Washburn, S. J.; Blum, J. D.; Kurz, A. Y.; Pizzuto, J. E. Spatial and Temporal Variation in the Isotopic Composition of Mercury in the South River, VA. *Chem. Geol.* **2018**, *494* (July), 96–108 DOI: 10.1016/j.chemgeo.2018.07.023.

(72) Yin, R.; Feng, X.; Hurley, J. P.; Krabbenhoft, D. P.; Lepak, R. F. Mercury Isotopes as Proxies to Identify Sources and Environmental Impacts of Mercury in Sphalerites. *Sci. Rep.* **2016**, November 2015, 1–8 DOI: 10.1038/srep18686.

(73) Yin, R.; Feng, X.; Shi, W. Application of the Stable-Isotope System to the Study of Sources and Fate of Hg in the Environment: A Review. *Appl. Geochemistry* **2010**, *25* (10), 1467–1477 DOI: 10.1016/j.apgeochem.2010.07.007.

(74) Yu, B.; Fu, X.; Yin, R.; Zhang, H.; Wang, X.; Lin, C.-J.; Wu, C.; Zhang, Y.; He, N.; Fu, P.; Wang, Z.; Shang, L.; Sommar, J.; Sonke, J. E.; Maurice, L.; Guinot, B.; Feng, X. Isotopic Composition of Atmospheric Mercury in China: New Evidence for Source and Transformation Processes in Air and in Vegetation. *Environ. Sci. Technol.* **2016** DOI: 10.1021/acs.est.6b01782.

(75) Zheng, W.; Demers, J.; Lu, X.; Bergquist, B. A.; Anbar, A. D.; Blum, J. D.; Gu, B. Mercury Stable Isotope Fractionation during Abiotic Dark Oxidation in the Presence of Thiols and Natural Organic Matter. *Environ. Sci. Technol.* **2018**, acs.est.8b05047 DOI: 10.1021/acs.est.8b05047.

(76) Zheng, W.; Hintelmann, H. Mercury Isotope Fractionation during Photoreduction in Natural Water Is Controlled by Its Hg/DOC Ratio. *Geochim. Cosmochim. Acta* **2009**, *73* (22), 6704–6715 DOI: 10.1016/j.gca.2009.08.016.

(77) Zheng, W.; Hintelmann, H. Isotope Fractionation of Mercury during Its Photochemical Reduction by Low-Molecular-Weight Organic Compounds. *J. Phys. Chem. A* **2010**, *114*, 4246–4253.

(78) Zheng, W.; Hintelmann, H. Nuclear Field Shift Effect in Isotope Fractionation of Mercury during Abiotic Reduction in the Absence of Light. *J. Phys. Chem. A* **2010**, *114* (12), 4238–4245 DOI: 10.1021/jp910353y.

(79) Zheng, W.; Obrist, D.; Weis, D.; Bergquist, B. A. Mercury Isotope Compositions across North American Forests. *Global Biogeochem. Cycles* **2016**, *30*, 1475–1492 DOI: 10.1002/2015GB005323.

Figures & Tables

Figure 1

Plot of δ^{202}Hg (‰) vs Δ^{199}Hg (‰) values for samples from the Yuba River watershed, including one site on the Feather River. Filtered surface waters (red circles) and suspended particulates (blue squares) were collected in June 2016, while values for biota (green triangles) and riverbank and terrace sediments (gray diamonds) taken from Donovan et al., 2016a, and were collected in 2013 and 2014.

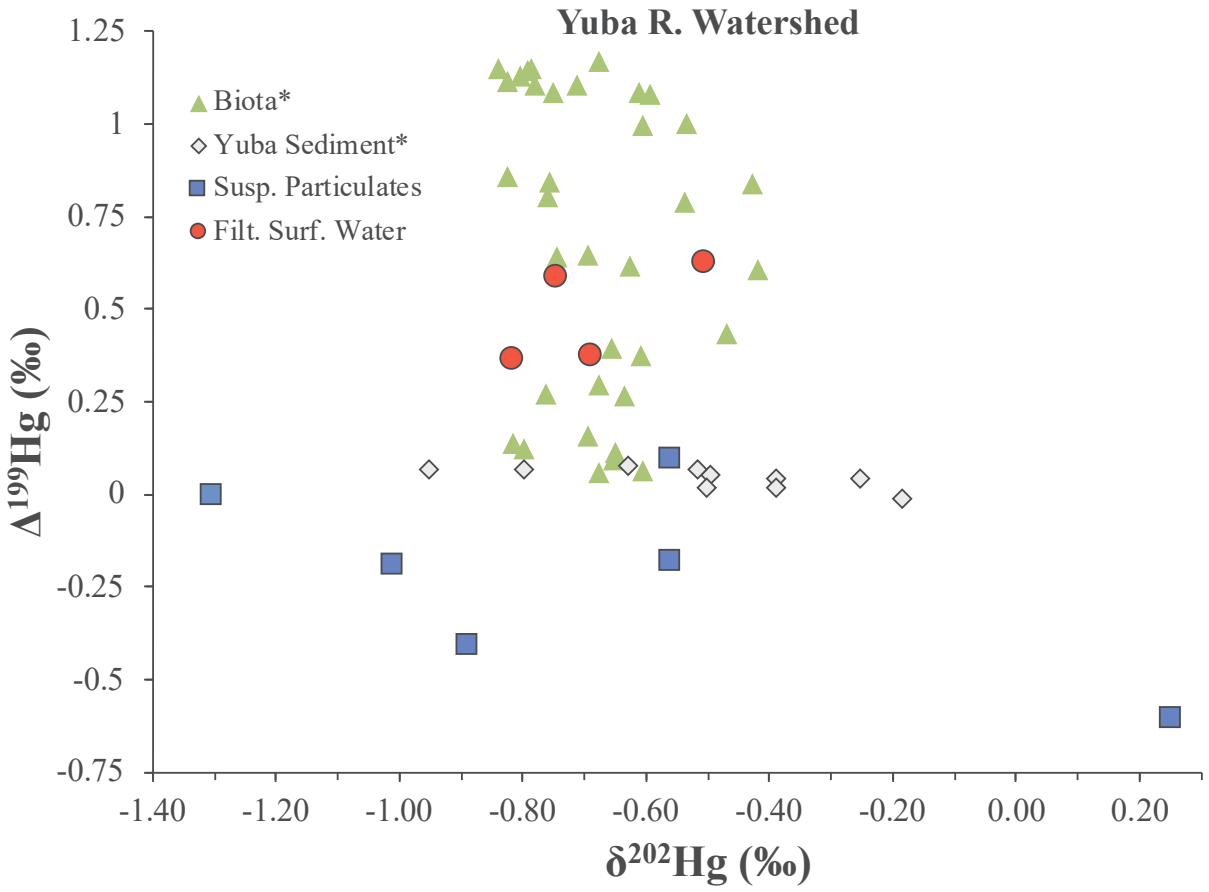

Figure 2
Plot of δ^{202}Hg (‰) vs Δ^{199}Hg (‰) values for samples from the Cache Creek watershed, including sites on Bear Creek and Sulfur Creek. Filtered surface waters (red circles) and suspended particulates (blue squares) were collected in June 2016, while values for biota (green triangles) and riverbed and terrace sediments (gray diamonds) taken from Donovan et al., 2016b, and were collected in 2013 and 2014. Note the difference in scales compared to Fig 1.

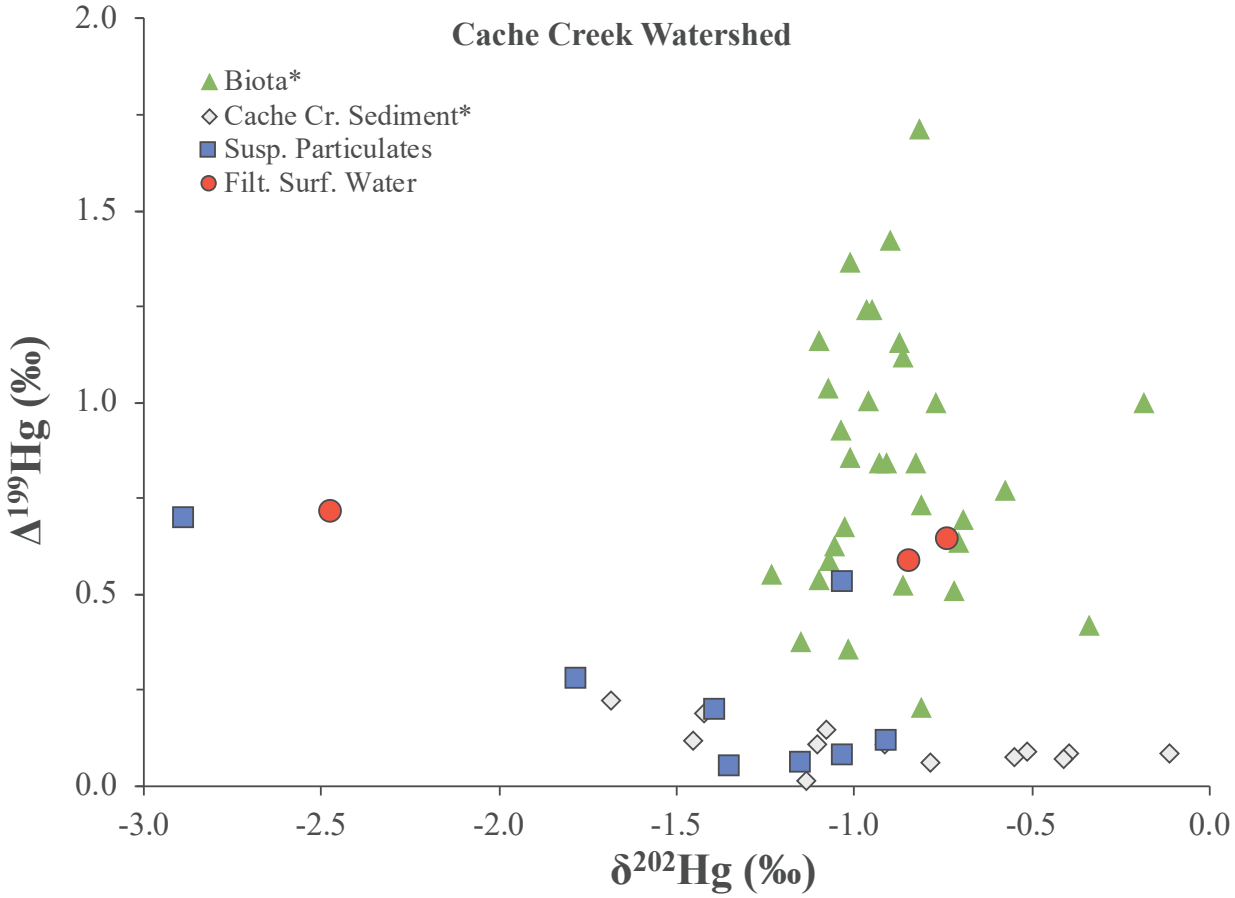

Figure 3
Plot of δ^{202}Hg (‰) vs Δ^{199}Hg (‰) values for paired riverbed and terrace sediments (diamonds), suspended particulates (squares), and filtered surface waters (circles). Samples from various sampling sites are denoted by the symbol color displayed in the figure legend. Sediment data taken from Donovan et al., 2016a and Donovan et al., 2016b.

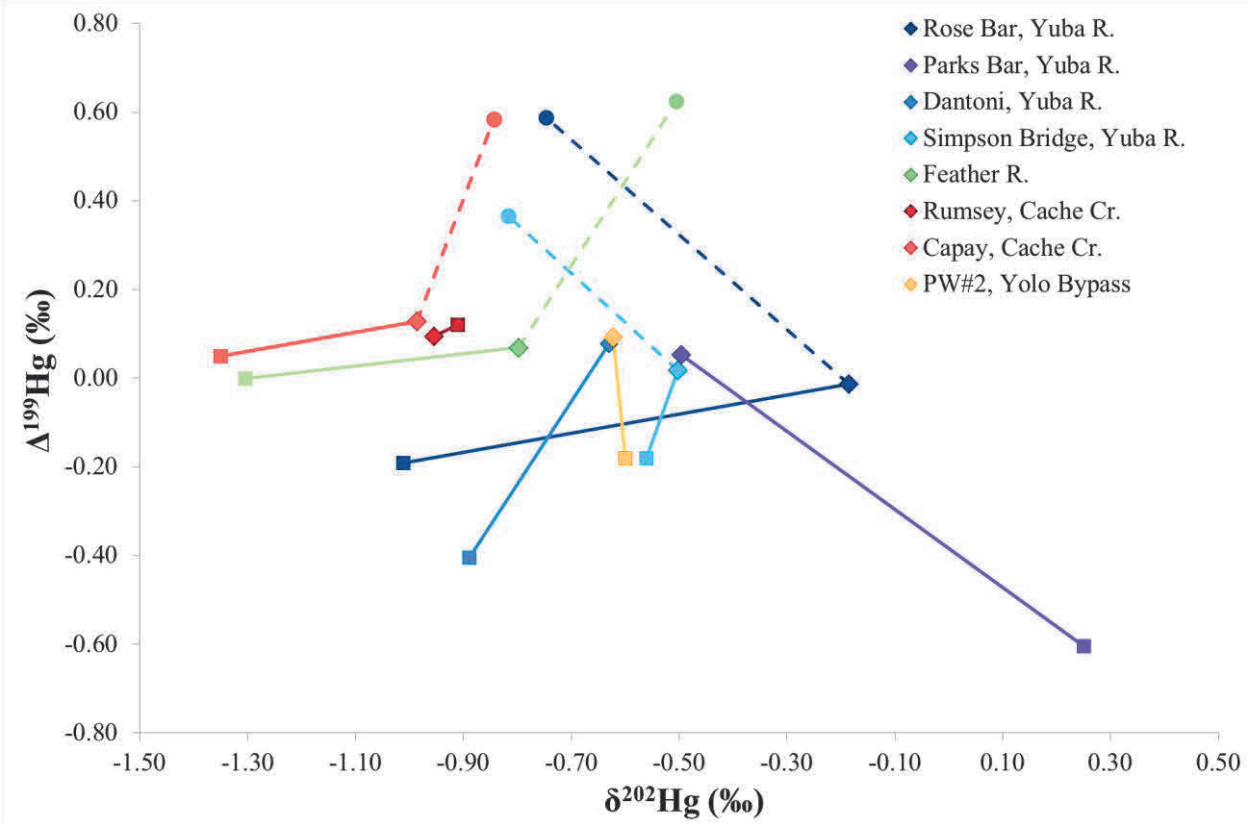

Figure 4

Plot of Δ^{201}Hg (‰) vs Δ^{199}Hg (‰) values for all filtered surface water samples (circles) and suspended particulates (squares) collected in both the Yuba River (red symbols), and Cache Creek (blue symbols) watersheds. The slope value for the combined watershed dataset (solid black line), only Cache Cr. dataset (solid blue line), and only Yuba R. dataset (solid red line), were calculated using a bivariate York regression (slope±2SE [shown as dotted black lines for combined slope]), as described in the text in Section 3.2.1. The two samples denoted with blue asterisks had low recoveries that were unlikely to affect MIF signatures but were not included in the linear regression calculations, as described in Section 2.2.

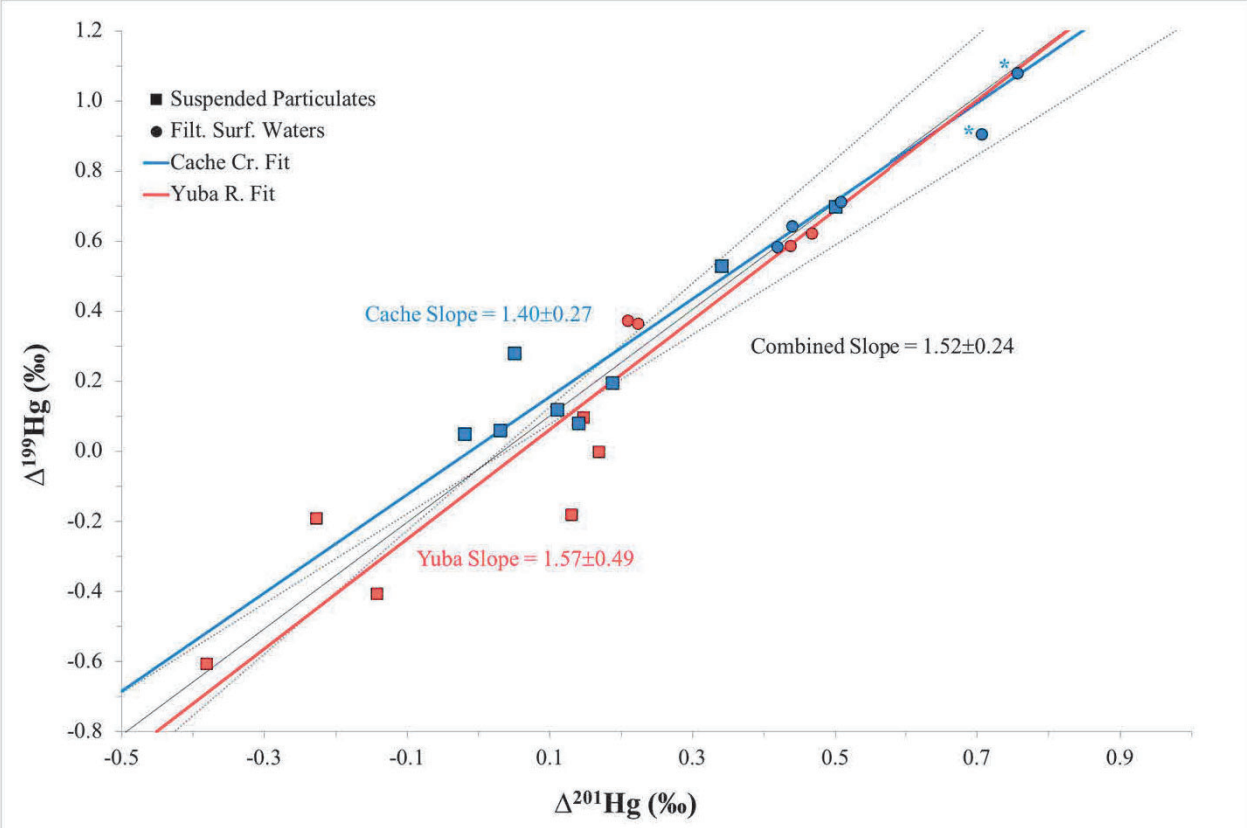

Table 1

Summary of THg concentration and Hg stable isotope data of collected samples from the CA Central Valley watersheds, including filtered surface waters ("FSW") and the associated suspended particulates ("SW Susp. Part.") from the Yuba R. and Cache Cr. watersheds and Yolo Bypass Wilderness Area. FSW samples denoted with ** (values highlighted in grey) had low recoveries that were unlikely to affect MIF signatures, but may have affected MDF signatures as discussed in Section 2.2

Watershed	Location	Sample Type	THg	THg	log(K_d)	δ^{204}Hg	δ^{202}Hg	δ^{201}Hg	δ^{200}Hg	δ^{199}Hg	Δ^{204}Hg	Δ^{201}Hg	Δ^{200}Hg	Δ^{199}Hg
			ng/L	ng/g		‰	‰	‰	‰	‰	‰	‰	‰	‰
Cache Creek	Bear Cr. Above Sulfur Cr.	SW Susp. Part.		1698.6	5.98	-2.48	-1.39	-0.86	-0.66	-0.15	-0.40	0.19	0.04	0.20
		FSW	1.77			-1.14	-0.73	-0.11	-0.33	0.46	-0.05	0.44	0.04	0.64
	Sulfur Cr.	SW Susp. Part.		57614.0	5.51	-4.39	-2.89	-1.67	-1.34	-0.03	-0.08	0.50	0.11	0.70
		FSW	179.08			-3.74	-2.47	-1.35	-1.18	0.09	-0.05	0.51	0.06	0.71
	Bear Cr. at Holston Chimney Canyon	SW Susp. Part.		2788.2	5.37	-1.52	-1.03	-0.43	-0.49	0.27	0.02	0.34	0.03	0.53
		**FSW	11.78			-2.28	-1.54	-0.40	-0.72	0.69	0.01	0.76	0.05	1.08
	North Fork Cache Cr.	SW Susp. Part.		210.7		-1.33	-1.03	-0.63	-0.52	-0.18	0.20	0.14	0.00	0.08
	Regional Park	SW Susp. Part.		114.6		-1.90	-1.15	-0.84	-0.57	-0.23	-0.18	0.03	0.01	0.06
	Rumsey	SW Susp. Part.		154.2	5.18	-1.44	-0.91	-0.57	-0.43	-0.11	-0.09	0.11	0.02	0.12
		**FSW	1.03			-1.59	-1.06	-0.09	-0.48	0.64	-0.02	0.71	0.05	0.91
	Guinda	SW Susp. Part.		223.3		-2.59	-1.78	-1.29	-0.82	-0.17	0.07	0.05	0.08	0.28
	Capay	SW Susp. Part.		472.0	5.44	-1.81	-1.35	-1.03	-0.62	-0.29	0.20	-0.02	0.06	0.05
		FSW	1.89			-1.28	-0.84	-0.22	-0.39	0.37	-0.02	0.42	0.03	0.58
Yuba River	Rose Bar	SW Susp. Part.		166.1	5.65	-0.92	-1.01	-0.99	-0.55	-0.45	0.59	-0.23	-0.04	-0.19
		FSW	0.48			-1.12	-0.75	-0.12	-0.34	0.40	-0.01	0.44	0.03	0.59
	Parks Bar	SW Susp. Part.		665.2		0.66	0.25	-0.19	-0.17	-0.54	0.29	-0.38	-0.29	-0.61
	HammonGrove	SW Susp. Part.		401.1	5.72	-0.94	-0.56	-0.28	-0.26	-0.04	-0.10	0.15	0.02	0.10
		FSW	0.86			-1.09	-0.69	-0.31	-0.34	0.20	-0.06	0.21	0.01	0.37
	Dantoni	SW Susp. Part.		612.4		-0.50	-0.89	-0.81	-0.72	-0.63	0.83	-0.14	-0.27	-0.41
	Simpson Bridge	SW Susp. Part.		361.3	5.71	-1.13	-0.56	-0.29	-0.29	-0.32	-0.29	0.13	-0.01	-0.18
		FSW	0.74			-1.22	-0.82	-0.39	-0.40	0.16	0.00	0.22	0.01	0.37
	Feather R.	SW Susp. Part.		238.3	5.62	-1.78	-1.31	-0.81	-0.62	-0.33	0.17	0.17	0.03	0.00
		FSW	0.57			-0.79	-0.50	0.09	-0.22	0.50	-0.04	0.47	0.03	0.62
Yolo Bypass Wilderness Area	Permanent Wetlands #2	SW Susp. Part.		222.0	5.23	-0.86	-0.60	-0.53	-0.42	-0.33	0.03	-0.09	-0.12	-0.18
		FSW	1.30			NA								

Table

Click here to download Table: Washburn_Table1.docx

Table 1

Summary of THg concentration and Hg stable isotope data of collected samples from the CA Central Valley watersheds, including filtered surface waters ("FSW") and the associated suspended particulates ("SW Susp. Part.") from the Yuba R. and Cache Cr. watersheds and Yolo Bypass Wilderness Area. FSW samples denoted with ** (values highlighted in grey) had low recoveries that were unlikely to affect MIF signatures, but may have affected MDF signatures as discussed in Section 2.2

Watershed	Location	Sample Type	THg	THg	log(K_d)	δ^{204}Hg	δ^{202}Hg	δ^{201}Hg	δ^{200}Hg	δ^{199}Hg	Δ^{204}Hg	Δ^{201}Hg	Δ^{200}Hg	Δ^{199}Hg
			ng/L	ng/g		‰	‰	‰	‰	‰	‰	‰	‰	‰
Cache Creek	Bear Cr. Above Sulfur Cr.	SW Susp. Part.		1698.6	5.98	-2.48	-1.39	-0.86	-0.66	-0.15	-0.40	0.19	0.04	0.20
		FSW	1.77			-1.14	-0.73	-0.11	-0.33	0.46	-0.05	0.44	0.04	0.64
	Sulfur Cr.	SW Susp. Part.		57614.0	5.51	-4.39	-2.89	-1.67	-1.34	-0.03	-0.08	0.50	0.11	0.70
		FSW	179.08			-3.74	-2.47	-1.35	-1.18	0.09	-0.05	0.51	0.06	0.71
	Bear Cr. at Holston Chimney Canyon	SW Susp. Part.		2788.2	5.37	-1.52	-1.03	-0.43	-0.49	0.27	0.02	0.34	0.03	0.53
		**FSW	11.78			-2.28	-1.54	-0.40	-0.72	0.69	0.01	0.76	0.05	1.08
	North Fork Cache Cr.	SW Susp. Part.		210.7		-1.33	-1.03	-0.63	-0.52	-0.18	0.20	0.14	0.00	0.08
	Regional Park	SW Susp. Part.		114.6		-1.90	-1.15	-0.84	-0.57	-0.23	-0.18	0.03	0.01	0.06
	Rumsey	SW Susp. Part.		154.2	5.18	-1.44	-0.91	-0.57	-0.43	-0.11	-0.09	0.11	0.02	0.12
		**FSW	1.03			-1.59	-1.06	-0.09	-0.48	0.64	-0.02	0.71	0.05	0.91
	Guinda	SW Susp. Part.		223.3		-2.59	-1.78	-1.29	-0.82	-0.17	0.07	0.05	0.08	0.28
	Capay	SW Susp. Part.		472.0	5.44	-1.81	-1.35	-1.03	-0.62	-0.29	0.20	-0.02	0.06	0.05
		FSW	1.89			-1.28	-0.84	-0.22	-0.39	0.37	-0.02	0.42	0.03	0.58
Yuba River	Rose Bar	SW Susp. Part.		166.1	5.65	-0.92	-1.01	-0.99	-0.55	-0.45	0.59	-0.23	-0.04	-0.19
		FSW	0.48			-1.12	-0.75	-0.12	-0.34	0.40	-0.01	0.44	0.03	0.59
	Parks Bar	SW Susp. Part.		665.2		0.66	0.25	-0.19	-0.17	-0.54	0.29	-0.38	-0.29	-0.61
	HammonGrove	SW Susp. Part.		401.1	5.72	-0.94	-0.56	-0.28	-0.26	-0.04	-0.10	0.15	0.02	0.10
		FSW	0.86			-1.09	-0.69	-0.31	-0.34	0.20	-0.06	0.21	0.01	0.37
	Dantoni	SW Susp. Part.		612.4		-0.50	-0.89	-0.81	-0.72	-0.63	0.83	-0.14	-0.27	-0.41
	Simpson Bridge	SW Susp. Part.		361.3	5.71	-1.13	-0.56	-0.29	-0.29	-0.32	-0.29	0.13	-0.01	-0.18
		FSW	0.74			-1.22	-0.82	-0.39	-0.40	0.16	0.00	0.22	0.01	0.37
	Feather R.	SW Susp. Part.		238.3	5.62	-1.78	-1.31	-0.81	-0.62	-0.33	0.17	0.17	0.03	0.00
		FSW	0.57			-0.79	-0.50	0.09	-0.22	0.50	-0.04	0.47	0.03	0.62
Yolo Bypass Wilderness Area	Permanent Wetlands #2	SW Susp. Part.		222.0	5.23	-0.86	-0.60	-0.53	-0.42	-0.33	0.03	-0.09	-0.12	-0.18
		FSW	1.30			NA								

Figure

Click here to download Figure: Washburn_Figure1.pdf

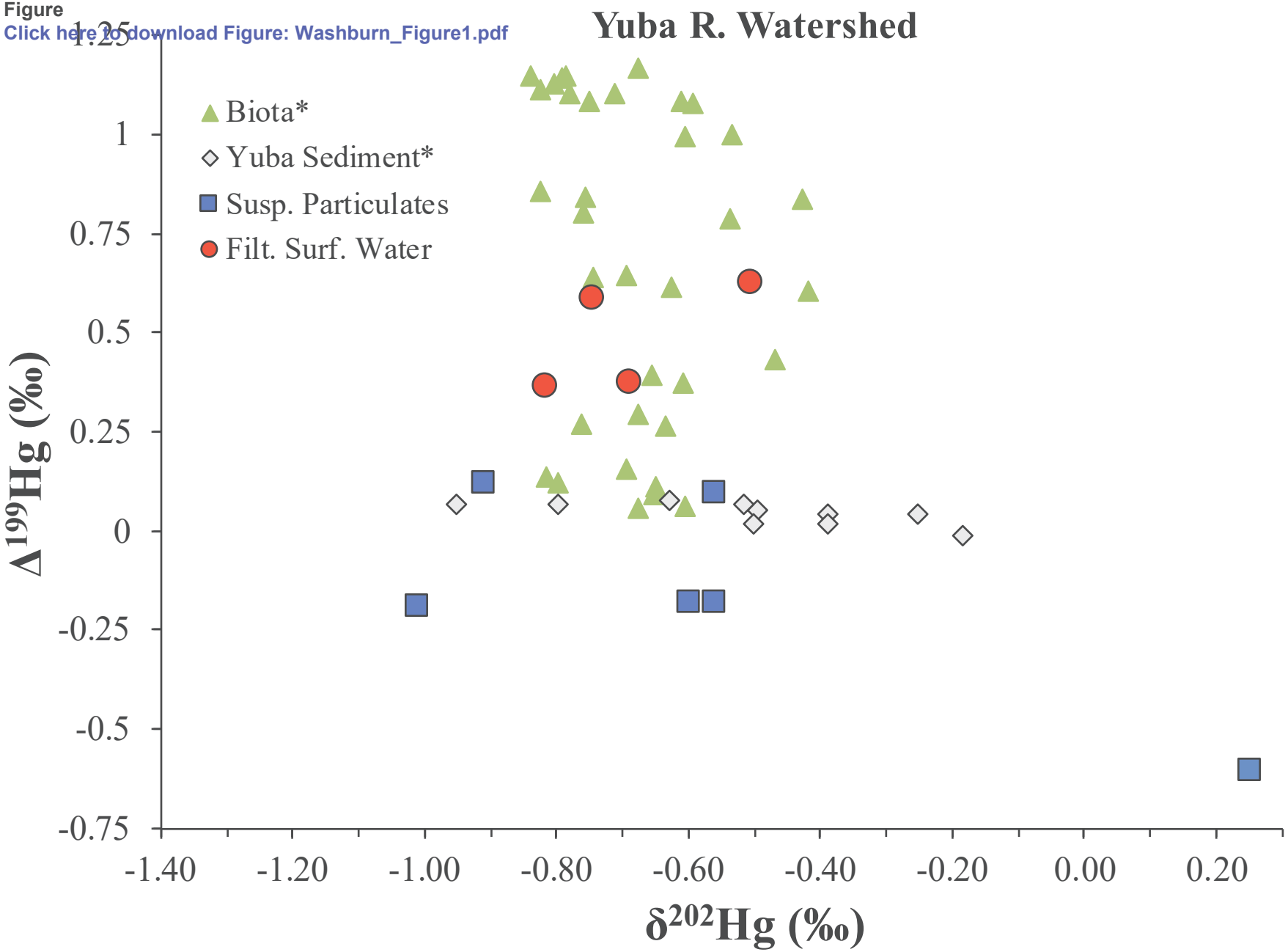

Figure

Click here to download Figure: Washburn_Figure2.pdf

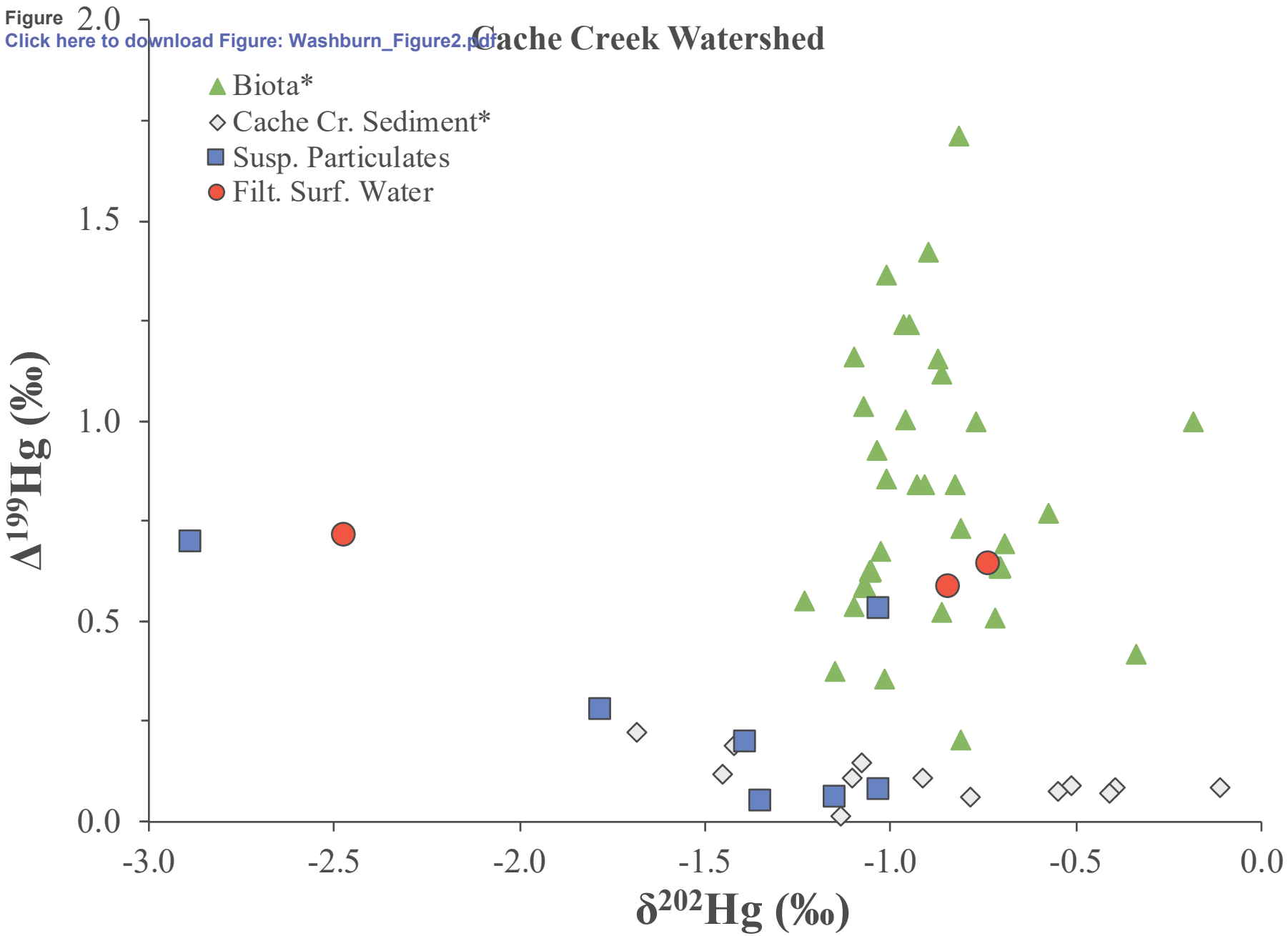

Figure
Click here to download Figure: Washburn_Figure3.pdf

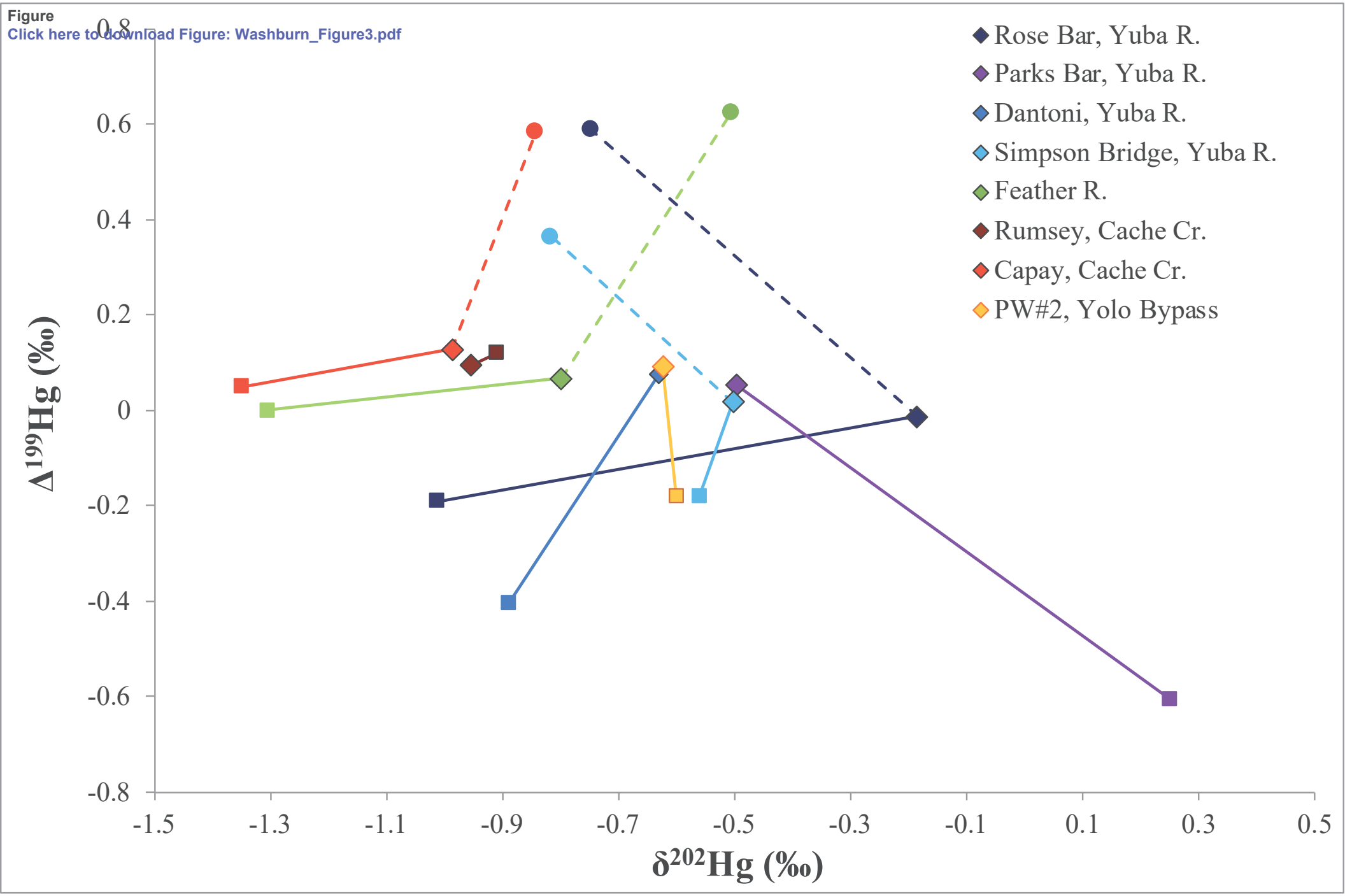

Figure
Click here to download Figure: Washburn_Figure4.pdf

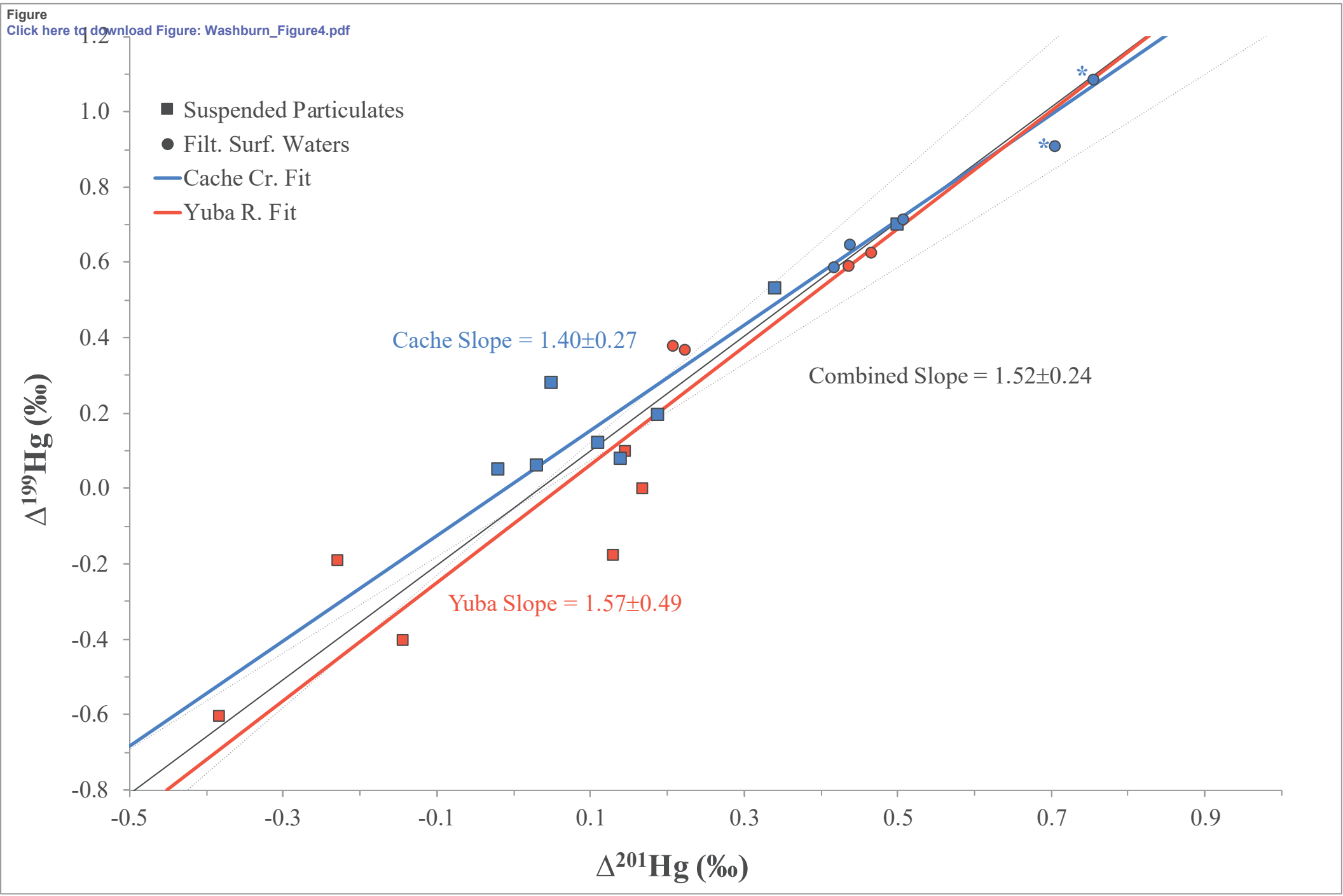

Supplementary material for on-line publication only

Click here to download Supplementary material for on-line publication only: SI_Washburnetal_CASurfaceWater_revised.docx